

Chapter 1

Localized Nonlinear Waves in Lattices

Abstract

In this chapter we will study the nonlinear behavior of atomic lattices coupled by realistic potentials. Essentially, in this conservative system the dispersion is caused by lattice periodicity, where the nonlinearity appears at the coupling between oscillators following a Coulomb type interaction. Thus, strongly supersonic localized waves can be generated and propagates along the lattice in the form of kinks. With the aim of study a more realistic physical system, we include a model accounting for nuclear repulsion effects that modifies the nonlinear interaction for short interatomic distances. In addition, we propose a substrate potential that modifies the lattice dispersion relation. The physical parameters are those of the K^+ ion lattice in a mica muscovite layered silicate.

1.1 Motivation: dynamics of potassium ions in layered silicates

Many minerals are known by their capability of recording the tracks of charged particles, and are often used as solid state nuclear track detectors (SSNTDs); a review of the subject can be found in Refs. (Durrani, 2001; Durrani, 2008).

Among them, mica muscovite has been relevant as it was the second material and the first natural one where tracks from fission fragments were found (Silk et al., 1959). Very soon later fossil tracks were also found in mica (Price et al., 1962). It seems to be one of the most sensitive of natural SSNTD (Fleischer, 2011). Due to its resistance to heat, it can be used inside a nuclear reactor core for particle detection. It has also been used in geochronology and to probe the existence of dark matter (Snowden-Ifft et al., 1995), to find exotic nuclear reactions, decays of superheavy elements and weakly interacting massive particles (WIMPs) (Durrani, 2001; Durrani, 2008). Micas have also important technological applications due their dielectric and heat shielding properties. Other uses are as matrixes for films, monochromators and dispersive crystals.

Silicates are also among the materials considered as engineered barriers for nuclear waste storage due to its high rate of reaction with heavy ions in low temperature reconstructive transformations (Alba et al., 2001). This property can be of importance for the development of advanced structural ceramics (Hong et al., 2002) and has been related to the existence of nonlinear localized vibrations related with the ones described in this work (Archilla et al., 2006; Dubinko et al., 2011).

Tracks of positrons, muons and other particles have been reported (Russell, 1967b; Russell, 1967a; Russell, 1988b; Russell, 1988a) in mica muscovite. Some of these tracks were identified as produced by positrons resulting from the $\beta+$ decay of ^{40}K. This isotope is relatively abundant in the minerals and can also experience $\beta-$, electron capture and other kind of decays. Most of the tracks, however, cannot be explained as being produced by charged particles but could have been produced by some kind of vibrational excitation because, among other properties, the tracks are along the close-packed lines of the K^+ hexagonal layer shown in Fig. 1.1. One interpretation of these tracks is that they are formed by the localized nonlinear excitations, sometimes called quodons (Schlößer et al., 1994), whose exact nature is still not known.

A likely source for the vibrational energy required to initiate a *quodon* is the recoil energy of the ^{40}K after β decay, which can be up to 52 eV. In muscovite, there are about 3 decays per second and cm^3, so after many years of the sensitive period, when tracks recording is possible, there are many possibilities to initiate a *quodon*. An experiment was done to shed some light into the relationship between tracks and *quodons* (Russell et al., 2007). A mica specimen was irradiated with alpha

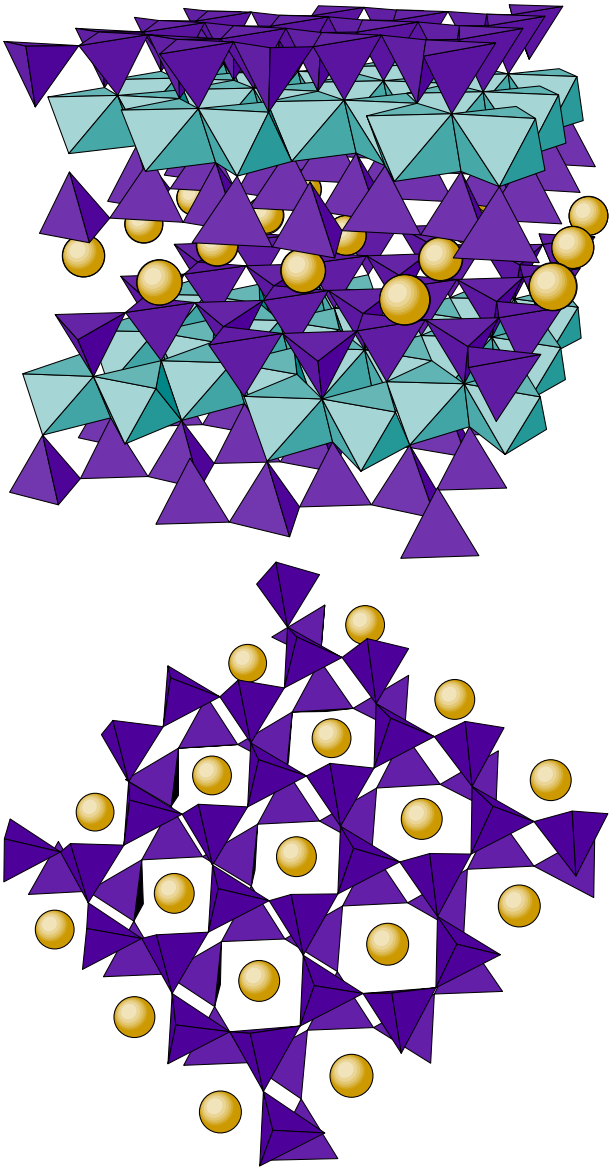


Figure 1.1: Representation of the mica structure from the point of view that emphasizes the close-packed lines of the K^+ hexagonal layer represented by yellow balls. Crystal structure of muscovite. The circles represent the potassium ions forming the interlayer sheet. The unit cell includes two silicate layers and two K^+ions with parameters $a = 5.19$Å, $b = 9.02$Å; $c = 20.0$ Å; and $\beta = 95.7^o$. For a view from the top, see the later Fig. 1.16

particles and the ejection of atoms was detected on the other side, along closed packed lines. The ejected atoms could not been identified and also sputtering energies are not known exactly, however from experimental and theoretical studies, they are known to be in the range of 4-8 eV (Kudriavtsev et al., 2005).

In an attempt to understand this phenomenon, numerical simulations were conducted in an idealized 1D model where the particles of increasing energy hit the boundary of the lattice (Dou et al., 2011). This study reports the formation of a breather and kinks and the ejection of atoms at the opposite boundary of the sample. However, the model did not intend to use realistic values of the mica muscovite parameters.

A minimal model of the cation lattice with realistic parameters was proposed recently (Archilla et al., 2013; Archilla et al., 2014). Only K^+ ions were considered with the actual potassium mass and Coulomb interaction between them. The interaction with the rest of the lattice was implicitly considered as the force keeping the ions inside the crystal with the known interatomic distance in muscovite. In those publications, it was reported the existence of supersonic kinks, which were easily generated within a wide range of energies and velocities.

However such model is too simplistic because for relatively high ion energies it results in unrealistically small distances between the ions, of tenths of angstrom.

In this chapter, we develop a dynamical model in which we use the Ziegler-Biersack-Littmark (ZBL) short-range repulsive potential, introduced in particle bombardment studies (Biersack et al., 2008). ZBL potential describes the Coulomb repulsion between nuclei, which is partially screened by the atom electrons and rapidly decays in few Å. The results for the moving energy-carrying objects in such potential are similar to those obtained with only pure Coulomb interaction (Archilla et al., 2013; Archilla et al., 2014), namely the supersonic kinks, traveling without attenuation for long distances, can be produced with arbitrary energies. But the inter-particle distances in the kinks are limited by physically reasonable values in our dynamical model. Note that our dynamical model allows for bond dissociation, which is a necessary condition for the realistic modeling of the normal energy transport in low-dimensional systems (Savin et al., 2014).

As a next step towards a more realistic description, we construct explicitly the interaction with the surrounding atoms, using standard empiric potentials introduced in molecular dynamics, which give rise to a periodic non-sinusoidal substrate potential. Supersonic lattice kinks, also called *crowdions* (Kosevich et al., 1973), are also easily obtained. They propagate in such potential with a velocity which is independent of the input and is determined only by the lattice potential parameters. For the smaller energies, the kink dissipates in phonons, while for larger energies the excess energy is radiated until reaching the value of crowdion energy.

The final crowdion energy is approximately 26 eV, which can be provided by

the recoil of isotopes of potassium after radioactive decay and is larger than the sputtering energy. This ratio of characteristic energies allows to assume that the tracks found in mica muscovite can be related with the lattice kinks or crowdions.

The literature about kink propagation in lattices with different inter-particle and on-site potentials is extensive. The most studied and generic model is the Frenkel-Kontorova (FK) model(Frenkel et al., 1938), see reviews in Refs. (Chaikin et al., 1995; Braun et al., 1998; Braun et al., 2004). However, most of the kinks considered in this model are subsonic ones. Supersonic kinks in the systems with substrate have been found in models with anharmonic intersite coupling (Kosevich et al., 1973; Milchev, 1990; Savin, 1995; Zolotaryuk et al., 1997). They have the property than only a discrete set of velocities allows the propagation of kinks without attenuation. They can be described as multi-kinks or lattice N-solitons depending on whether the description is done in terms of coordinates, strains or velocities. The kink with the unique supersonic velocity, propagating in our dynamical model of the cation layer on a substrate, is a double-kink.

The FK model has also been considered in layered materials, to model, for example, the in-plane dynamics of a few-layer graphene, in order to explain molecular dynamics simulation results for the cross-plane thermal conductance (Ni et al., 2014). One particular characteristic, found in the kinks studied in the present work, is extreme discreteness of the kinks, namely only two particles, and for higher energies, practically only one particle is in motion at a given time. This discreteness allows the complete understanding in physical terms of the mechanism that brings about a single velocity of the kink and why the kink is a double-kink.

The Chapter is organized as follows. First we review and extend the results obtained with only the Coulomb interaction, using the sinusoidal waveform proposed for supersonic kinks in the Fermi-Pasta-Ulam (FPU) lattice (Kosevich, 1993; Kosevich et al., 2004). The sinusoidal waveform is a good description for $\lambda \simeq 3a$, where λ is a characteristic wavelength of the sinusoidal waveform and a is a lattice constant, but fails for $\lambda \simeq 2a$, been replaced by an almost triangular waveform, corresponding to nearly hard-sphere collisions. Afterward we consider the effects of long-range interactions, with several neighbours, and introduce a short-range nearest-neighbor ZBL potential. Thereafter, the substrate potential is constructed and the properties of the single-velocity lattice kinks in the cation layer on the substrate are analyzed with details.

1.2 Minimal model with realistic potentials

1.2.1 Model

We consider as a starting point a one-dimensional (1D) model for the dynamics of K^+ions. Thus, considering nearest-neighbour Coulomb interaction the position,

x_n, of each n-th atom is given by

$$m\frac{\partial^2 x_n}{\partial t^2} = -\frac{\mathrm{K_C e^2}}{(x_{n+1}-x_n)^2} + \frac{\mathrm{K_C e^2}}{(x_n - x_{n-1})^2}, \tag{1.1}$$

where m is the K^+mass, $\mathrm{K_C e^2}$ is the inter-ion Coulomb electrostatic constant. With the aim of explore solutions from a more general approach, we can write the equation in dimensionless form by choosing as unit of distance, $a = 5.19$ Å(i.e. the lattice constant or the equilibrium distance between K^+ ions; for masses, the mass of a K^+ ion, $m_{K^+} = 39.1$ amu; for time, $\tau = \sqrt{m_K a^3/\mathrm{k_e\, e^2}} \simeq 0.2$ ps, where $\mathrm{k_e}$ is the Coulomb constant and e is the elementary unit of charge. Other physical units in the system are velocity $u_V = 2600$ m/s, energy $u_E = 2.77$ eV and frequency 5 THz. Dimensionless speed of sound in this system is $c_0 = \sqrt{2}$, or about 3.700 km/s in physical units.

Thus, defining u_n as the displacement with respect to the equilibrium position normalized to the lattice constant, witch can be expressed as $x_n = a(n + u_n)$, the dimensionless motion equations become

$$\frac{\partial^2 u_n}{\partial t^2} = -\frac{1}{(1+u_{n+1}-u_n)^2} + \frac{1}{(1+u_n-u_{n-1})^2}, \tag{1.2}$$

which describes the chain of ions coupled to their nearest neighbours by electrostatic Coulomb potential. Note hereinafter t will be dimensionless time.

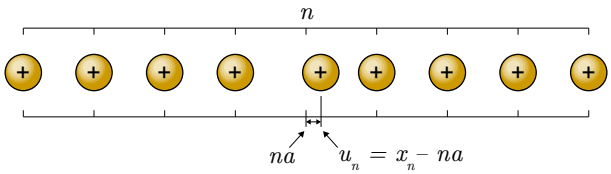


Figure 1.2: Scheme of the one dimensional model of the K^+ ion layer

1.2.2 FPU equivalent lattice

For small amplitudes, the potentials in Eq. (1.2) can be expanded in a series, using that $1/(1+y)^2 \simeq 1 - 2y + 3y^2 - 4\,y^3 \ldots$. Retaining cubic and smaller terms, we obtain

$$\begin{aligned}\frac{\partial^2 u_n}{\partial t^2} \;=\; & c_0^2\,[(u_{n+1}+u_{n-1}-2u_n) \\ & -3/2\,(u_{n+1}-u_n)^2 + 3/2\,(u_n-u_{n-1})^2 \\ & +2\,(u_{n+1}-u_n)^3 - 2\,(u_n-u_{n-1})^3 + \ldots],\end{aligned} \tag{1.3}$$

which are the α-β FPU equations of motion. We would like to emphasize that the α-β FPU Eq. (1.3) describes the Coulomb lattice (1.2) only in the small- and intermediate-amplitude limit and is not applicable to this lattice in the large-amplitude limit, see Fig. 1.9 and the subsection devoted to the triangular waveform below.

1.2.3 Dispersion relations

Linearization Eq. (1.2), i.e. setting $\alpha = \beta = 0$ in Eq. (1.3), the equation of motion is reduced to the well-known discrete linear wave equation

$$\frac{\partial^2 u_n}{\partial t^2} = c_0^2 \ (u_{n+1} + u_{n-1} - 2u_n)\,, \tag{1.4}$$

where c_0, the speed of sound, is the long wavelength phonon velocity. Note that in our scaling $c_0 = \sqrt{2}$. A phonon corresponds to small amplitude particle displacements of the form $u_n = \exp\left(i\left(qn - \omega t\right)\right)$, with q and ω being the phonon wave number and frequency respectively. The dispersion relation and velocities are well known, we include them here for comparison with. Thus, the the phonon dispersion equation in normalized units reads

$$\omega^2 = 4c_0^2 \sin^2 \frac{q}{2} \quad \text{with} \quad q = \frac{2\pi m}{N} \quad \text{and} \quad m = 1, 2, \ldots, N. \tag{1.5}$$

Then, phase and group velocity are expressed for the lattice as

$$\begin{aligned} c_p &= \frac{\omega}{q} = 2c_0 \left| \frac{\sin \frac{q}{2}}{q} \right|, \\ c_g &= \frac{\partial \omega}{\partial q} = c_0 \left| \cos \frac{q}{2} \right|. \end{aligned} \tag{1.6}$$

Thus, those well known relations dispersion of the linear lattice and its group and phase velocity velocity are plotted for the positive first Brillouin zone in Fig. 1.3. The maximum frequency corresponding to the mode with the wave number $q = \pi$ is $\omega_M = 2c_0$. In the limit of long wavelengths, both velocities are equal to the speed of sound c_0, which is also the maximum value. Note that the group velocity becomes zero at the top of the phonon band $q = \pi$.

The maximum frequency in physical units is about 2.2 THz which is larger than the one obtained with molecular dynamics and neutron spectroscopy of about 1.6 THz (Collins et al., 1993; Wada et al., 1991; Chaplot et al., 2002). This is understandable given the simplicity of our model taking into account just one type of atom compared with the complexity of real mica, but it is within the same range of values. Note that the predicted speed of sound in physical units, $c_0 = 3690.2$ m/s, is similar to that found in Ref. (Brudeylins et al., 1995) of 3400-3700 m/s.

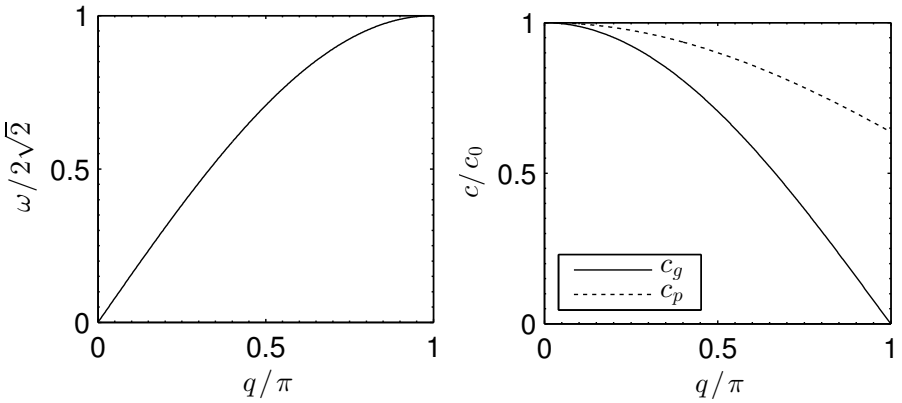


Figure 1.3: Left: Dispersion relation for the linearized Coulomb lattice. Right: Phase speed and group velocity for linearized Coulomb lattice. In the limit of long wavelengths, both give the sound velocity, which can be compared with the values of 3.4–3.7 km/s obtained in Ref. (Brudeylins et al., 1995)

Also note that, in contrast with the *repulsive* character of the full Coulomb interaction, this linearized equation is *attractive*, i.e. if the distance $u_{n+1} - u_n$ increases, the force on the particle u_n is positive. The reason for it is the decreasing nature of the Coulomb force: when the distance with the particle in front increases the repulsion weakens and the repulsion from the particle behind becomes larger pushing the particle n forward.

1.3 Tail analysis

Different types of nonlinear localized solutions are supported by the Coulomb lattice. Although these solutions are large enough to be intrinsically nonlinear, they also have tails of small amplitude which abide the linear equation. Tails cannot exist by themselves but depends on the existence of the nonlinear solution, however its study gives information about the parent excitation. We obtain first the tail properties and later we consider the fully nonlinear solutions. Tails are obtained with the linear system, therefore their properties are common to any system with the same linearization. However, they only give the conditions that the tails have to fulfill. The properties of existence of the nonlinear excitation, its velocity, amplitude and other characteristics have to be worked out with the whole nonlinear system.

Consider a nonlinear localized moving excitation, travelling with velocity V. We also assume that its amplitude decays exponentially far away enough from the

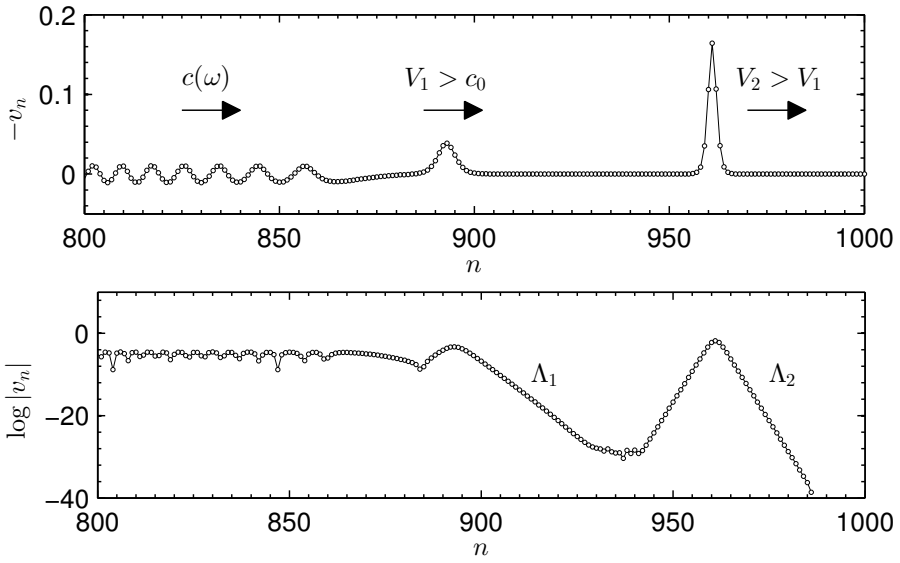


Figure 1.4: Numerical example of two nonlinear localized waves travelling at different velocities and leaving a phonon tail. (Top) profiles obtained at fixed time. (Bottom) logarithmic representation showing that front and back tails exist with different decay length. Despite the type of the excitation and its nonlinear features, the tail analysis predict the relation between the parent velocity and its localization, i.e. $V_i(\Lambda_i)$.

center. Tails are well described by the expression

$$u_n = \exp\left(-\xi\left(n - Vt\right)\right)\exp\left(\mathrm{i}\left(qn - \omega t\right)\right)\,, \tag{1.7}$$

where $|\xi|$ is the localization parameter and its inverse $\Lambda = 1/|\xi|$ the decay length. This equation is valid for $n > Vt$ if $\xi > 0$ and it corresponds to the front tail of the structure, where for $n < Vt$ if $\xi < 0$ corresponding to the back tail. The limit case $\xi = 0$ corresponds to extended phonons. Figure 1.4 shows an example were two localized waves are numerically obtained presenting different tails and velocities.

Since the tail amplitude is by definition small, it satisfies the linear equation Eq. (1.4). Using that $u_{n+1} = \exp(-\xi + \mathrm{i}q)u_n$, $u_{n-1} = \exp(\xi - \mathrm{i}q)u_n$ and $\dot{u}_n = (\xi V - \mathrm{i}\omega)u_n$, substitution of (1.7) in (1.4) yields the following two equations:

$$\begin{aligned} \xi^2V^2 - \omega^2 &= 2c_0^2(\cosh(\xi)\cos(q) - 1) \\ \xi V\omega &= c_0^2\sinh(\xi)\sin(q)\,. \end{aligned} \tag{1.8}$$

As there are two equation with four unknowns, we can express two of them as ω and V as functions of the other two ξ and q. First, the frequency ω is given by:

$$\omega = \cosh(\xi/2)2c_0\sin(q/2) = \cosh(\xi/2)\omega_{\text{phonons}}\,. \tag{1.9}$$

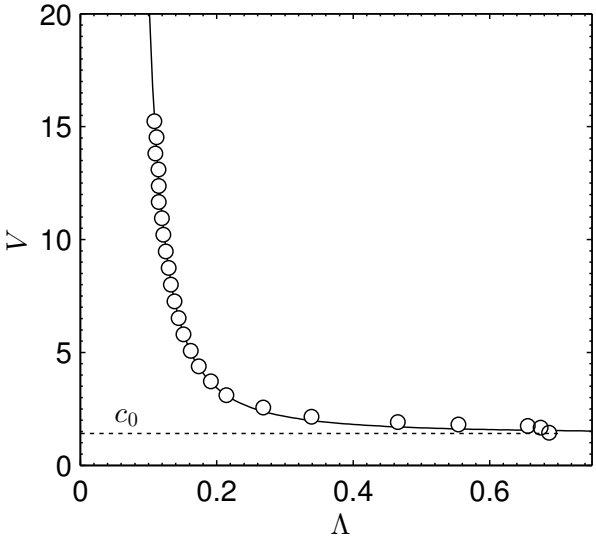


Figure 1.5: Comparison of the numerical (circles) and theoretical (continuous line) decay lengths as a function of the velocity for a localized wave (kink). Dimensionless units

Note that Eq. (1.9) reduces to the phonon dispersion equation when there is no localization, i.e. $\xi \to 0$.

The velocity of the tail of the hypothetical localized wave is given by:

$$V = \frac{\sinh(\xi/2)}{\xi/2}\, c_0 \cos(q/2) = \frac{\sinh(\xi/2)}{\xi/2} c_g \,. \tag{1.10}$$

The relationship between the decay length $\Lambda = 1/|\xi|$ and V given by the equation above is in excellent agreement with the numerical results, as can be seen in Fig. 1.5. Note that both $\sinh(\xi/2)/(\xi/2)$ and $\cosh(\xi/2)$ are larger than the unity and also monotonically increasing functions in $|\xi|$, which means that the tails oscillate and move faster than the phonons. Except for the degenerate case $\xi = 0$, which corresponds to no localization and no tail, i.e., to phonons. Essentially, the conclusion that arise for the tail analysis states that localized travelling waves, either solitons or kinks, with tails following Eq. (1.7) are supersonic, where its velocity depends on the localization. Also note this analysis was developed with the linearized discrete wave equation and does not depend of the specific nonlinearity of the coupling. Is thus generic for many systems of coupled oscillators. However, for studying the specific features of localized nonlinear travelling waves in the Coulomb lattice the nonlinear terms can not be neglected.

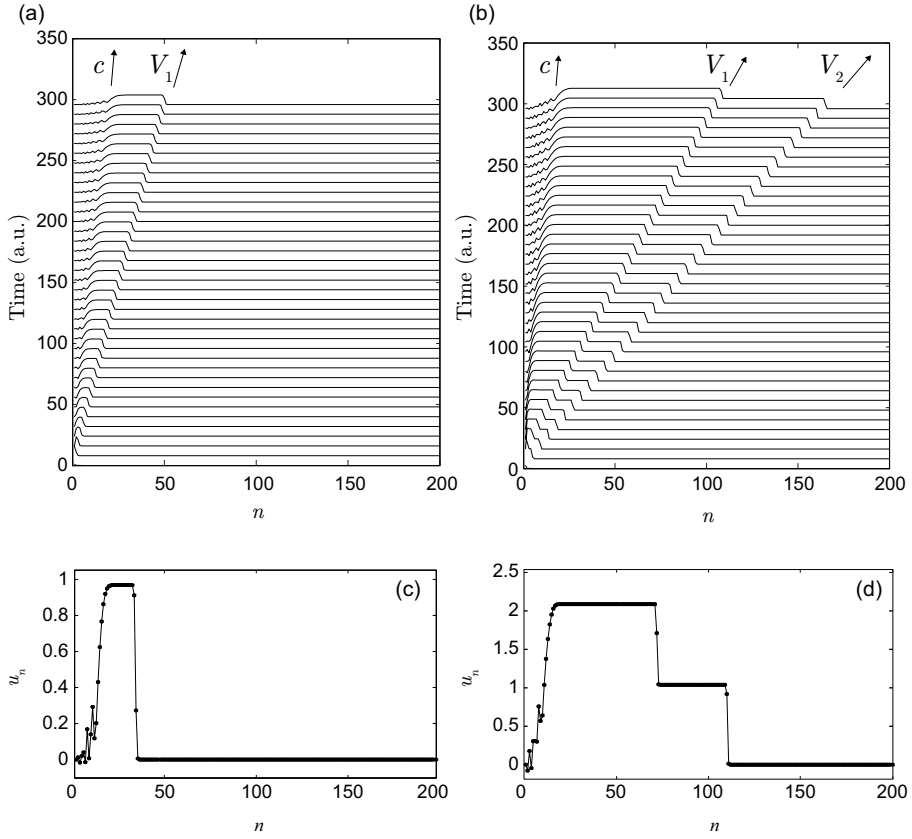


Figure 1.6: (a) Profile and evolution of a single kink for initial amplitude $A_0 = 1.05$. (b) Excitation of multikinks for initial amplitude $A_0 = 2.5$ where two kinks with different velocities are observed. (c,d) Detail of the corresponding displacements at $t = 200$ scaled units. A tail of phonons is left behind the localized travelling nonlinear waves.

1.4 Supersonic ultra-discrete kinks

1.4.1 First supersonic kinks and multi-kinks

We propose the study of kink solutions in the lattice. Essentially, a kink is a nonlinear localized wave that connects and divide two phases of the domain. Kinks can be stationary or propagating. We find that the simplified proposed model for the repulsive lattice is extremely well suited for propagation ultra-discrete supersonic kinks and multi-kinks. Due to the analytical analysis of the kink characteristics will be somehow restricted, a numerical integration of the complete set of equations of motion has been used to explore the full nonlinear features of the lattice.

The numerical evaluation of the Eq. (1.2) retaining the exact form of the Coulomb type interaction is trivial using centered finite differences with a "leap-frog" time marching scheme. Thus, for one-dimensional lattices of $N < 1000$ elements and the integration times considered on this Chapter, the temporal step required can be small enough to achieve convergence and the error due to numerical dispersion can be controlled for all simulations.

Thus, the boundary conditions for the simulations are set to fix at rest the first and last atoms of the chain, i.e. those conditions implicitly includes the effects of the other atoms of the mica crystal in the simplest way, forcing the central part of the chain to remain at rest. Then, a excitation is forced in one extreme of the chain. As a first example, as in Ref. (Kosevich et al., 2004), the first particle in the chain is forced to move sinusoidally during half a period, with an amplitude A_0, so that the initial and final positions are both zero (more details of this waveform will be given in following sections). Increasing the amplitude of the perturbation A_0 the velocity of the kink increases, and eventually, two, three, and any number of kinks are produced, travelling one after the other. The dependency of the velocity and number of kinks with the initial amplitude is shown in Fig. (1.6) for one (a, c) and for two (b, d) kinks.

1.4.2 Test solution

In order to obtain the properties of the full nonlinear system it is convenient to introduce a new variable, the deformation from the equilibrium position or *strain* $v_n = u_n - u_{n-1}$, the equations above can be written as:

$$\frac{\partial^2 v_n}{\partial t^2} = 2F_n - F_{n+1} - F_{n-1}; \quad \text{with} \quad F_n = \frac{1}{(1+v_n)^2}, \tag{1.11}$$

where $v_n = 0$ corresponds to the unperturbed lattice. The boundary conditions assume fixed particles at the ends of the lattice. Kinks are produced numerically by applying at the chain boundary a *half-wave* perturbation, which is a sinusoidal displacement during half of a period, starting and finishing at the equilibrium position (Archilla et al., 2013; Kosevich et al., 2004). In order to describe a kink traveling to the right, the following *ansatz* was introduced as in Refs. (Kosevich, 1993; Kosevich et al., 2004):

$$v_n = -\frac{A}{2}\left(1 + \cos\left(qn - \omega t\right)\right) \quad \text{if} \quad -\pi \leq qn - \omega t < \pi, \tag{1.12}$$

and $v_n = 0$ otherwise, where A is the kink strain amplitude. The bonds are always compressed so v_n is negative with a minimum value of $-A$, corresponding to the maximum compression of the bond. For analogy, we use the usual wave terminology, so $\phi_n = \omega t - q\, n$ is the phase; q is the wave number; ω is the angular

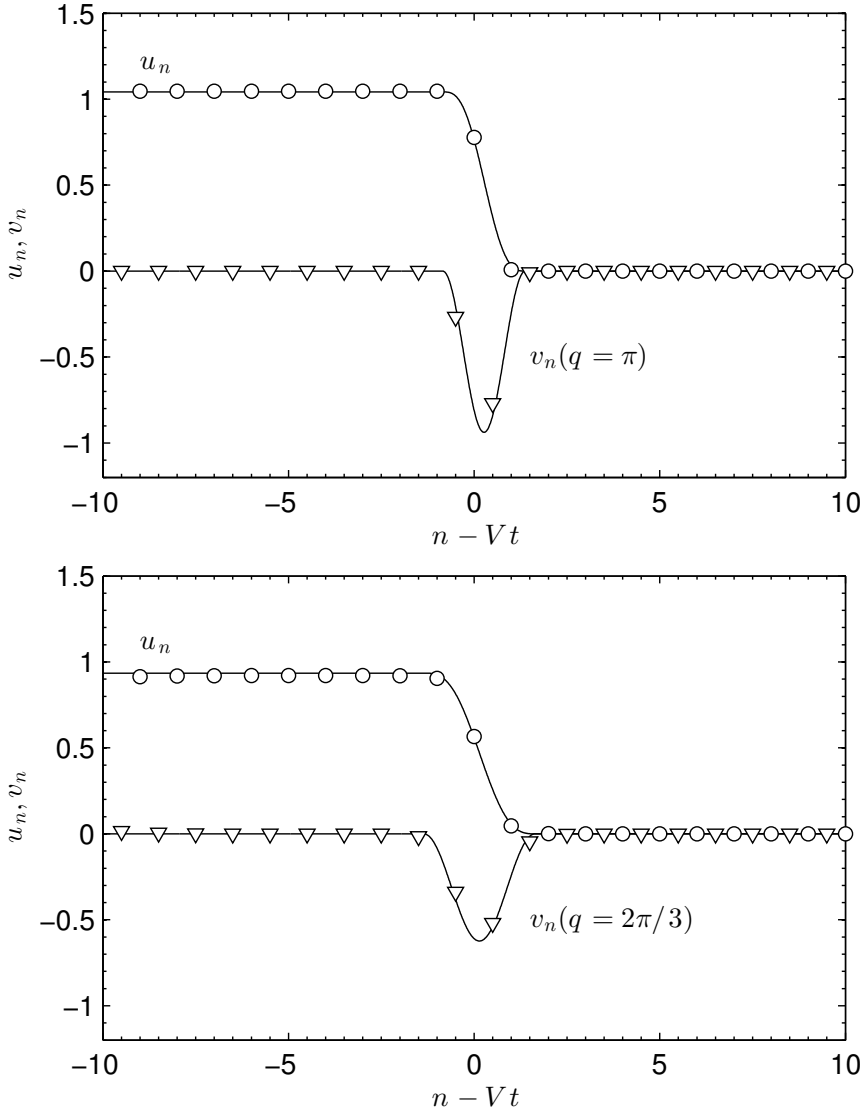


Figure 1.7: Spatial profile at fixed time for kinks represented in displacement (u_n) and strains $v_n = u_n - u_{n-1}$. Circles and triangles are numerical results and the continuous lines are obtained from Eq. (1.12) with *magic* wave number $q \simeq 2\pi/3$ (top), when basically two particles are moving at a given time, and with $q \simeq \pi$ (bottom) for the amplitude A close to 1, when basically one particle is moving at a given time. Scaled units are equal to the lattice unit.

frequency; T is the period; $\lambda = 2\pi/q$ is the wavelength. The sinusoidal waveform with $q = 2\pi/3$, being an exact solution for the FPU lattice(Kosevich, 1993; Kosevich et al., 2004), is not an exact solution for the Coulomb lattice but is a good approximation for intermediate values of the amplitude A and provides very useful framework for understanding the relative phases of the particles and the behavior of the kink.

Figure 1.7 (top) compares the result of the numerical simulation for displacements and strains, with the corresponding analytical expressions derived from Eq. (1.12), for the intermediate value of the amplitude $A = 0.55$ and wave number $q \simeq 2\pi/3$. The analytical expression fits very well the numerical data. Figure 1.7 (bottom) pictures a kink with wavenumber $q = \pi$. There are not enough particles to compare with the analytical form, but the main properties of the latter are valid.

For the dimensionless wave number $q = 2\pi/\lambda$, with λ an integer, Eq. (1.12) represents a solution where basically λ bonds and $\lambda - 1$ particles (the kink core) are in motion, while the others remain at rest.

We will use the term *active* to describe related states of the different magnitudes. The active particles or coordinates at a given time or time interval (or phase or phase interval) are those for which u_n is changing, the active bonds are those for which $v_n \neq 0$, i.e., they are the compressed ones. For a particle, the time interval is active when it is moving, and for a bond - when it is compressed.

If the dimensionless wavelength λ is between two integers m_1 and m_2, the number of active bonds oscillates between m_1 and m_2 and the number of active oscillating particles is between $m_1 - 1$ and $m_2 - 1$.

Of particular interest in this work will be $\lambda = 3$, with $q = 2\pi/3$, which is called the *magic wave number* (Kosevich et al., 2004), and $\lambda = 2$, with $q = \pi$, which will be referred to as the π-mode. These two values are extreme cases of localization, with $q = \pi$ being the limit when only one particle is moving at a given time.

1.4.3 Rotating wave approximation

The velocities of the kinks can be analytically obtained using the rotating wave approximation (RWA), which consists in an approximation of the Fourier series up to the first harmonic (Archilla et al., 2013). When we substitute (1.12) in the equation of motion (1.11), nonlinearity generates multiple frequencies. The RWA approximation states that nonlinear contributions higher than second harmonics can be neglected. This implies that the force terms can be approximated by their first-order Fourier expansions, as $F_n = a_0 + a_1 \cos(qn - \omega t)$. On the other hand, the left hand side of Eq. (1.11) gives, after substitution of Eq. (1.12), $\ddot{v}_n = (A/2)\omega^2 \cos(qn - \omega t)$ which is equal to the first harmonic term of the right hand side. The zero-harmonic cancels out due to the dependency of the right hand

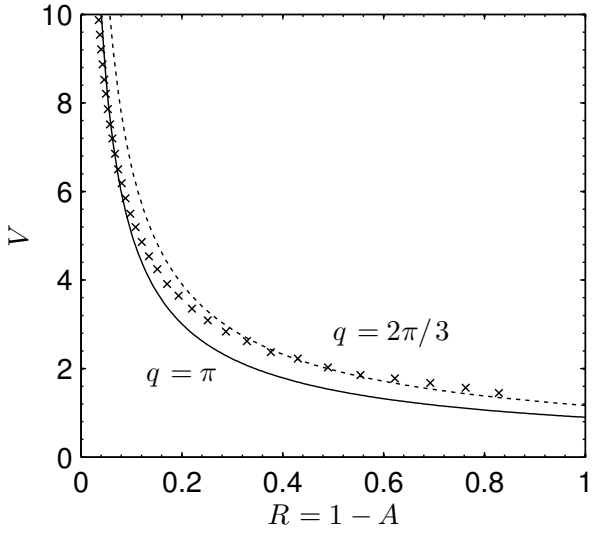


Figure 1.8: Kink velocity versus minimal interparticle distance $R = 1 - A$, calculated numerically (crosses) and analytically from Eq.(1.15) with wave number $q = 2\pi/3$ (upper dotted-dashed line) and $q = \pi$ (lower dotted-dashed line). Scaled units are the lattice constant for distances and 2.6 km/s for velocities.

side on F_n. The first harmonic of F_n is given by:

$$a_1 = \frac{1}{\pi}\int_{-\pi}^{\pi} \frac{\cos(\theta)\mathrm{d}\theta}{(1-\frac{A}{2}-\frac{A}{2}\cos(\theta))^2}\,. \tag{1.13}$$

For $A < 1$ we obtain

$$a_1 = \frac{A}{(1-A)^{3/2}}. \tag{1.14}$$

Therefore, substituting $\ddot{v}_n$ and $F_n = a_0 + a_1\cos(qn - \omega t)$ in Eq. (1.11), is straightforward to obtain the frequency as a function of the amplitude A:

$$\omega = \frac{1}{(1-A)^{3/4}}\, 2c_0 \sin\left(q/2\right), \tag{1.15}$$

and the velocity as:

$$V = \frac{1}{(1-A)^{3/4}}\; c_0\; \frac{\sin\left(q/2\right)}{(q/2)}. \tag{1.16}$$

Kinks are therefore supersonic. These magnitudes are equal to the corresponding ones for phonons, multiplied by a amplitude factor $1/(1-A)^{3/4}$: in the small

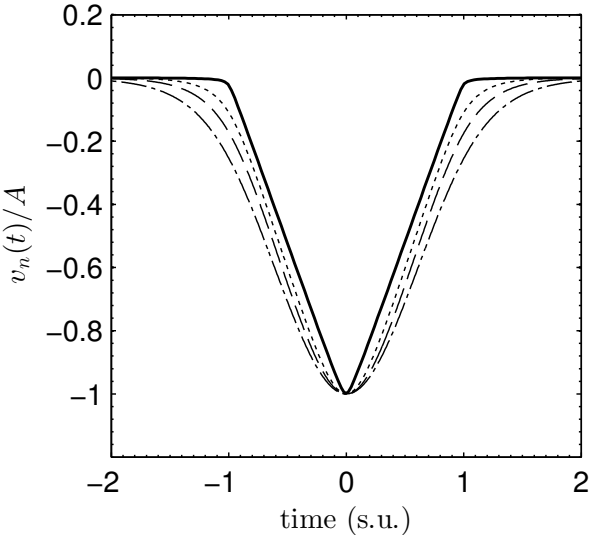


Figure 1.9: Temporal variation of the strain $v_n = u_n - u_{n-1}$ for different amplitudes. As the amplitude A increases, the shape becomes almost triangular, corresponding to almost hard-spheres collisions. The amplitude A is given in lattice units and the scaled time unit is 2 ps.

amplitude ($A \to 0$) and long wavelength ($q \to 0$) limit, V tends to the sound speed c_0.

In Ref. (Archilla et al., 2013) it was shown that the magic wave number represents a good agreement between the *ansatz* and simulations. However this agreement fails at the kink amplitudes A approaching unity, when the minimal interparticle distance in the kink (in lattice units) $R = 1 - A$ diminishes and the $q = \pi$ brings about a much better fit as can be seen in Fig. 1.8. The conclusion is that the magic wave number is a suitable approximation for an intermediate range of amplitudes in the Coulomb lattice, in contrast to the FPU chain where it is valid for all amplitudes(Kosevich, 1993; Kosevich et al., 2004), and that q actually changes continuously with the amplitude in the Coulomb lattice. The complementary approach is to use Eq. (1.15) to find the values of the wave number q, with respect to the amplitude A or the velocity V. This will be shown in Fig. 1.14, where it can be appreciated that the magic wave number is a satisfactory solution only for the intermediate values of kink velocity in the Coulomb lattice.

1.4.4 Triangular waveform

For the higher amplitudes, with A close to 1, the waveform deviates from the sinusoidal one given by Eq. (1.12) and approaches instead the triangular waveform, which is shown in Fig. 1.9. The almost straight lines in such waveform mean that

the velocity is almost constant except during a very short interaction time. The system behavior is very similar to that of the hard-spheres model.

This waveform is also another way of looking at the mode $q = \pi$. In this mode only one particle is moving at a given time, which means that there are no forces on the particle acting from its neighbours (because it moves at constant velocity and those forces would accelerate it). Strictly speaking, the mode $q = \pi$ and an exact triangular waveform are unattainable because of the electrostatic Coulomb forces acting on the particles. However, if the energy of the particle is large with respect to the change in the potential during a large part of the path between collisions, the particle will move almost free during most of the time between collisions.

The triangular waveform has been described as the high-energy limit for the Lennard-Jones interatomic potential (Friesecke et al., 2002) and has been observed experimentally in a system of repelling magnets (Molerón et al., 2014). It is worth mentioning that the triangular waveform can also be related with strongly-stretched bonds in the high-energy limit in the potentials allowing for bond dissociation, like the Lennard-Jones potential. The strongly-stretched bonds result in finite (normal) thermal conductivity in one-dimensional systems with such interatomic potentials (Savin et al., 2014).

1.4.5 Analytical results

Sinusoidal waveform and mode with $q = 2\pi/3$

Some analytical results can be obtained in this model, see also (Kosevich et al., 2004). Let us consider the wavenumber $q = 2\pi/3$ and choose $t = 0$ for the time for which $\phi_n = q\,n - \omega t = 0$ at $n = 0$ after a change of the origin of n and t, but keep the notation n for generality. If we consider the time interval Δt: $-T/6 \leq t < T/6$, there are three active strains: v_{n+1}, v_n and v_{n-1}. At the end of the interval, that is at $t = T/6$, v_{n-1} becomes zero and v_{n+2} starts being perturbed, so all the indexes n of the particles will change in a unity.

During Δt, $u_{n'} = 0$ for $n' \geq n + 1$, u_n and u_{n+1} are changing but u_{n-1} has already attained the value $3A/2$, its final constant value as can be checked by direct sum of 1.12 for $q = 2\pi/3$. Also, $u_{n'} = 3\,A/2$ for $n' < n - 1$, their final value after the kink has passed over them as seen in Fig. 1.7. The active coordinates are therefore $u_n = -v_{n+1}$ and $u_{n-1} = -v_n + v_{n+1}$, i.e. the mode $q = 2\pi/3$ states that essentially two particles are moving at same time and there are tree active bounds.

After some algebra we get

$$\begin{aligned} u_n &= \frac{A}{2} + \frac{A}{2}\cos\left(\phi_n + 2\pi/3\right) \\ u_{n-1} &= A - \frac{A}{2}\cos\left(\phi_n - 2\pi/3\right) . \end{aligned} \tag{1.17}$$

We can obtain immediately the kink kinetic energy as $K = \frac{1}{2}\dot{u}_n^2 + \frac{1}{2}\dot{u}_{n-1}^2$, which results in

$$K = \frac{\omega^2 A^2}{8}\left(1 + \frac{1}{2}\cos\left(2\phi_n\right)\right) , \tag{1.18}$$

with maximum value

$$K_M = \frac{\pi^2}{12} V^2 A^2 . \tag{1.19}$$

The potential energy, with respect to the equilibrium state, is given by:

$$U = \frac{1}{1+v_{n-1}} + \frac{1}{1+v_n} + \frac{1}{1+v_{n+1}} - 3 . \tag{1.20}$$

By substitution, it can be seen that the maximum potential energy corresponds to the bond n at its maximum compression, i.e., with $\phi_n = 0$, while the bonds $n-1, n+1$ have a phase difference of $\pm 2\pi/3$ with a strain $u_{n-1,n+1} = -A/2\left(1 + \cos\left(\pm 2\pi/3\right)\right) = -A/4$. Therefore the maximum energy becomes:

$$U_M = \frac{1}{1-A} + \frac{2}{1-A/4} - 3 . \tag{1.21}$$

There is also a minimum potential energy which corresponds to the limit, in which only two bonds are different from zero with phases $\pm\pi/3$ and strain $v_n = -3A/4$. The minimum energy becomes

$$U_m = \frac{2A}{1-3A/4} - 2 . \tag{1.22}$$

Therefore the kink for the mode $q = 2\pi/3$ has always some compression energy U_m above the ground state.

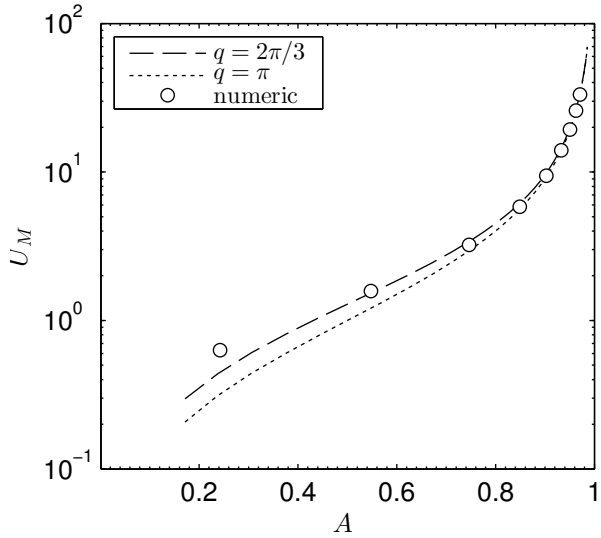


Figure 1.10: Maximum potential energies of the kinks in the Coulomb potential versus minimal interparticle distance in lattice units $R = 1 - A$ (for amplitude A close to 1). The analytical results are very similar for the waveforms with $q = \pi$ and $q = 2\pi/3$, as the maximum potential energy of the kink depends mainly on the minimal separation between particles R. The values of the dimension units are the lattice unit and 2.77 eV respectively.

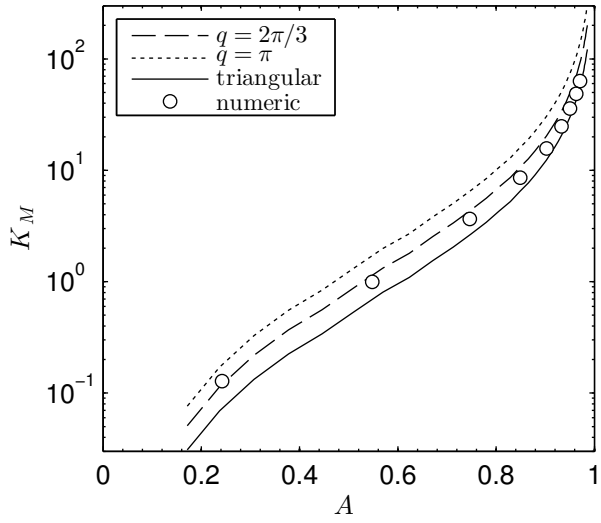


Figure 1.11: Maximum kinetic energies of the kinks in the Coulomb potential versus minimal interparticle distance in lattice units $R = 1 - A$ (for amplitude A close to 1). It can be seen that the kink with wavenumber π is better described by a triangular waveform than by a sinusoidal one. The values of the dimension units are the lattice unit and 2.77 eV respectively.

Sinusoidal waveform and mode with $q = \pi$

The properties of sinusoidal kinks with mode $q = \pi$ are easy to obtain as there are only two active strain variables and one coordinate, which during the interval $\Delta_\pi t$, $0 \le t < T/2$, are:

$$\begin{aligned} v_n &= -\frac{A}{2}\left(1+\cos\left(q\,n-\omega t\right)\right); \\ v_{n+1} &= -\frac{A}{2}\left(1+\cos\left(q[n+1]-\omega t\right)\right) = \\ &\quad -\frac{A}{2}\left(1-\cos\left(q\,n-\omega t\right)\right); \\ u_n &= -v_{n+1}\ ; \quad \dot{u}_n = \frac{A}{2}\omega\sin\left(q\,n-\omega t\right). \end{aligned} \tag{1.23}$$

The kinetic and potential energies, $K = \frac{1}{2}\dot{u}_n^2$ and $U = \dfrac{1}{1+v_n} + \dfrac{1}{1+v_{n+1}} - 2 = \dfrac{1}{1+v_n} + \dfrac{1}{1-v_n} - 2$, can be obtained. The maximum kinetic, maximum and minimum potential energies are given by

$$K_M = \frac{\pi^2}{8}A^2V^2\ ;\ U_M = \frac{1}{1-A} - 1\ ;\ U_m = \frac{2}{1-A/2} - 2. \tag{1.24}$$

Triangular waveform and mode with $q = \pi$

The potential energy fits very well the numerical values, unlike the kinetic energy, as can be seen in Figs. 1.10 and 1.11. This is because the π kink is better described by a triangular waveform in the limit of large energies, as Fig. (1.9) shows. Let us suppose that $t = 0$ is the time for which $v_n = -A$, as it takes half a period to change from $-A$ to 0, then $VT/2 = 2$. Therefore, for the interval $0 \le t < T/2$ the active variables for a ideal triangular waveform are:

$$\begin{aligned} v_n &= -A + AVt; \qquad & v_{n+1} &= -AVt; \\ u_n &= -v_{n+1} = AVt; \qquad & \dot{u}_n &= AV. \end{aligned} \tag{1.25}$$

The maximum and minimum potential energies are identical to that of the $q = \pi$ sinusoidal waveform given by Eq. (1.24).

On the other hand, the kinetic energy is a constant:

$$K = K_M = \frac{1}{2}A^2V^2\,. \tag{1.26}$$

In the numerical simulations, there are short time intervals when K changes, separated by a larger interval when K is almost constant.

In the high energy limit, $A \to 1$, the numerical solution converges to the triangular waveform: at fixed time only one particle is in movement, and its velocity is constant. During $0 < t < T/2$ the potential energy in this limit is negligible compared with the kink kinetic energy. Only when $t \to 0$ and $t \to T/2$ the moving particle *see* the Coulomb potential of the adjacent particles at rest. For $t \to T/2$ the particle experiment a deceleration, that in the limit $A \to 1$ can be considered as a rigid collision and therefore the kinetic energy must vanish for $t \to 0$ and for $t \to T/2$. Here a sharp peak on the potential energy is observed, where in the high amplitude limit a Dirac $\delta(t)$ is expected for energy conservation considerations.

Also, this result has implications in the interpretation of the kink as a particle-like excitation for high energies. In the limit $A \to 1$ the kink travels trough the lattice at constant velocity and energy, E, fixed by Eq. (1.26) as $E = \frac{1}{2}V^2$, which means that the kink behaves itself as a quasiparticle of unit mass (or a K^+ion mass in physical units).

1.5 Interaction with several neighbours

All the previous results apply to the case of nearest-neighbor coupling. However, for a more realistic description the long range interaction must be taken into account. With multiple neighbours, M, the dynamical equations become:

$$\frac{\partial^2 u_n}{\partial t^2} = \sum_{m=1}^{M} \left(-\frac{1}{\left(m + u_{n+m} - u_n\right)^2} + \frac{1}{\left(m + u_n - u_{n-m}\right)^2} \right), \tag{1.27}$$

which linearized become:

$$\frac{\partial^2 u_n}{\partial t^2} = c_0^2 \sum_{m=1}^{M} \frac{1}{m^3} \left(u_{n-m} - 2u_n + u_{n+m}\right). \tag{1.28}$$

Substitution of $u_n = \exp\left(\mathrm{i}\left(qn - \omega t\right)\right)$, leads to:

$$-\omega^2 u_n = c_0^2 \sum_{m=1}^{M} \frac{1}{m^3} \left(\exp\left(-\mathrm{i}qm\right) - 2 + \exp\left(\mathrm{i}qm\right)\right) u_n \tag{1.29}$$

with $c_0 = \sqrt{2}$, or:

$$\omega^2 = 4c_0^2 \sum_{m=1}^{M} \frac{1}{m^3} \sin^2\left(\frac{qm}{2}\right). \tag{1.30}$$

The function $\omega = \omega\left(q\right)$ is quite similar to the one with a single neighbour, but with a slope at $q = 0$ that increases with the number of neighbours. The phase

and group velocity are plotted in Fig. for the positive first Brillouin zone (1.12) for $M = 1, 3, 8, 50$. It is worth noting here that close to the continuous limit, i.e. $q \to 0$, $\sin(qm/2) \simeq qm/2$ and we obtain:

$$\omega^2 = q^2 c_0^2 \sum_{m=1}^{M} \frac{1}{M}. \tag{1.31}$$

Which leads to the group velocity at $q \to 0$ and $\lambda \to \infty$ $c_M = \partial\omega/\partial q$

$$c_M = c_0 \sqrt{\sum_{m=1}^{M} \frac{1}{m}}. \tag{1.32}$$

For a finite number of neighbours, the speed of sound is larger than with a single one. For example $c_3 = 1.354 c_0$ and $c_8 = 1.6486 c_0$. Note if causality is not imposed $\lim_{M\to+\infty} c_M = \infty$, although the convergence of is slow, e.g. for $M = 10^6$ neighbours $c_M = 3.7938 c_0$.

Simulation results show that kinks still exist and propagate supersonically when the Coulomb interaction extends beyond the nearest neighbours. Kinks have similar velocity and wave number if we normalize kink velocity to the sound speed in the Coulomb chain with interactions between M nearest neighbours, i.e. V/c_M.

Figure 1.13 shows the dependence of the relative velocity V/c_p on the minimum interparticle distance and Fig. 1.14 shows the dependence of the numerical best fit for the wave number as a function of the relative velocity, emphasizing the essential identity of the phenomenon. Other aspects of these figures will be commented below. For clarity, only the cases of three and eight neighbours are represented although up to 30 neighbours have been tested.

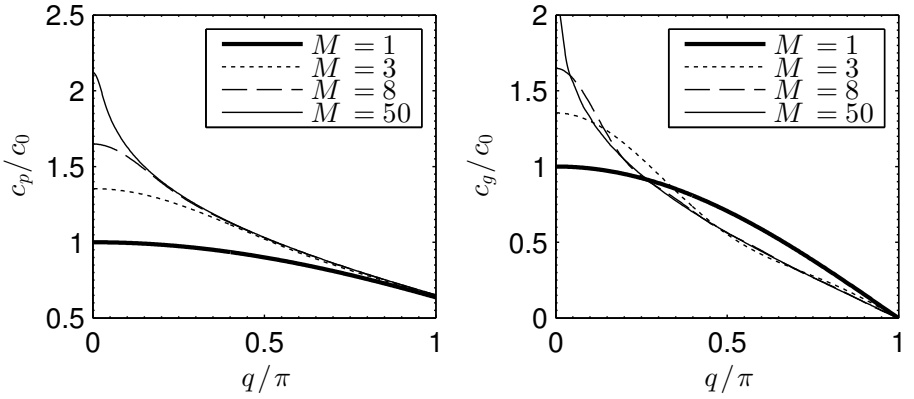


Figure 1.12: (left) Phase and (right) group velocity for the linearized Coulomb lattice including M=[1, 3, 8 and 50] neighbours.

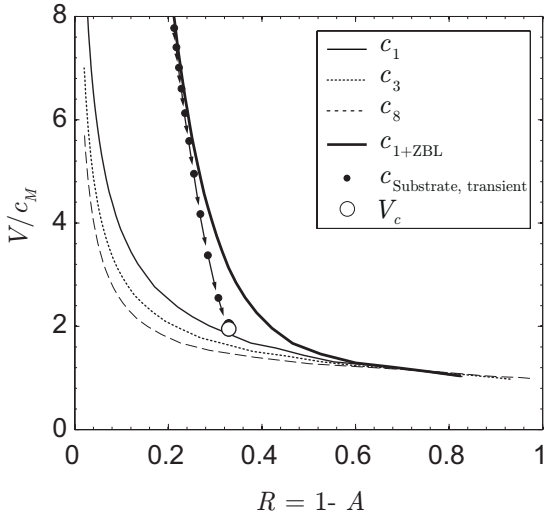


Figure 1.13: Kink velocities as a function of minimal interatomic distance in lattice units $R = 1 - A$ (A is kink's amplitude) for several potentials. Notations in the legend: c_m, $m = 1, 3, 8$, refers to the Coulomb interaction between the first m neighbours. Velocities are normalized to the sound speed c_M for a system with interaction between M neighbours, except for the system with a substrate which is normalized to $c_1 = c_s$. It can be seen that the increase of the number of interacting neighbours slows the normalized velocity V/c_M of the kink (but not its absolute velocity). Also, it can be seen that in the system with a substrate the normalized velocity V/c_M deviates from the curve $c_{1+\mathrm{ZBL}}$ to some specific velocity V_c on the c_1 curve. The values of the sound velocities are $c_1 = c_s = 3.7$ km/s, $c_3 = 5.0$ km/s and $c_8 = 6.1$ km/s.

It is worth commenting the problem that arises when the interaction with an infinite number of neighbours is taken into account. If the pair potential depends on the interparticle distance $|r|$ as $1/|r|^s$, the long-wave phonon velocity is finite for $s > 1$, but it diverges with the number of particles N as $v_{\mathrm{ph}} \propto \sqrt{\ln(N/2)}$ for the unscreened Coulomb potential ($s = 1$). However, this divergence occurs only in the electrostatic limit when the electromagnetic wave retardation is neglected. With an account of the retardation, the long-wave group velocity tends to the speed of light in vacuum. If the particles are in a material medium, there is a rearrangement of the electron density that can be described as a screening of the Coulomb interaction with some characteristic length l_{scr}. The screening brings about a finite long-wave phonon velocity $v_{\mathrm{ph}} \propto \sqrt{\ln(l_{\mathrm{scr}}/a)}$, where a is the lattice constant. As it has been mentioned, we do not study in depth this problem here and have considered only a few neighbours for simplicity.

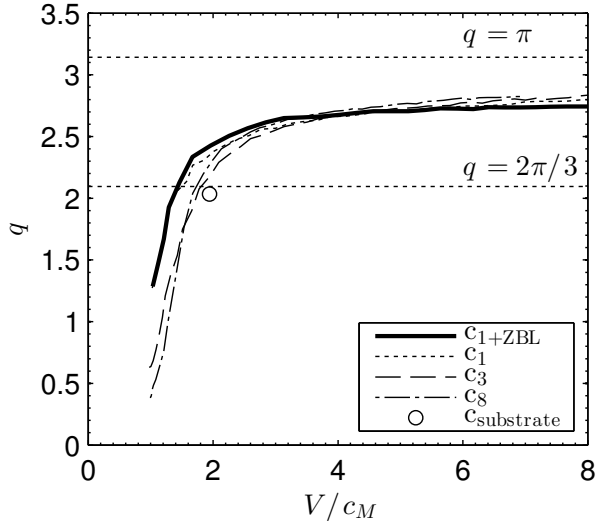


Figure 1.14: Best fit for the wavenumber q of the kinks as a function of the velocities normalized to the sound speed. Notations in the legend: C_i is the Coulomb interaction between the first i neighbours. Note that the *magic wave number* $q = 2\pi/3$ is also chosen in the system with a substrate. The values of the sound velocities are $c_1 = c_s = 3.7$ km/s, $c_3 = 5.0$ km/s and $c_8 = 6.1$ km/s.

1.6 The effect of nuclear repulsion: kinks with short–range ZBL potential

The minimal interatomic distance in lattice units $R = 1 - A$, obtained for fast large-amplitude kinks, is clearly impossible in realistic systems. At short distances short–range forces appear, which are produced by the overlapping electronic shells of the two close atoms. A large number of different repulsive potentials and screening functions have been proposed over the years, some determined semi-empirically, others from theoretical calculations. Much used repulsive potential is the one given by Ziegler, Biersack and Littmark, the so-called ZBL repulsive potential. It has been constructed by fitting a universal screening function to theoretically obtained potentials calculated for a large variety of atom pairs (Biersack et al., 2008). The ZBL potential has the form

$$U_{\mathrm{ZBL}}(r) = \mathrm{k_e}\,\frac{Z_1\,Z_2\,\mathrm{e}^2}{r}\,\phi\left(\frac{r}{\rho}\right)\,, \tag{1.33}$$

with $\mathrm{k_e}$ being the Coulomb constant, Z_1 and Z_2 are the atomic numbers of the involved atoms, and r the distance between them, $\phi(x)$ is the universal screening

Constant	$i=1$	$i=2$	$i=3$	$i=4$
A_i	0.1818	0.5099	0.2802	0.02817
b_i	3.2	0.9423	0.4029	0.2016

Table 1.1: Constants used for the Ziegler-Biersack-Littmark (ZBL) screening potential of Eq. (1.34)

function:

$$\phi(x) = \sum_{i=1}^{4} A_i \exp\left(-b_i x\right), \tag{1.34}$$

where the constants A_i and b_i are listed in Table (1.1).

The screening length is $\rho = 0.8854\, a_0 / \left(Z_1^{0.23} + Z_2^{0.23}\right)$, with $a_0 = 0.529$Å being the Bohr radius. The ZBL potential describes well the interaction between neutral atoms. In the case of ions considered here, the Coulomb potential must also be added, accounting for the repulsion between the ions. The introduction of the ZBL potential restricts the interatomic distances to the realistic values. The four terms in the ZBL potential are important for different range of energies, but for K^+ions, with energies up to 200 KeV, which are much larger that the ones considered here, the interaction potential can be represented by a single term, which together with the Coulomb ionic part takes the form:

$$U\left(r\right) = \frac{1}{r} + \frac{\alpha}{r} \exp(-\frac{r}{\rho}), \tag{1.35}$$

with $\alpha = 184.1$ and $\rho = 0.0569$ in dimensionless units, which in physical units correspond to 2650.6 eVÅand 0.29529 Å, respectively. Figure 1.15 represents ZBL and Coulomb potentials, with their sum and other details to be commented later. Note that around $r \simeq 0.4$, the combined potential $U(r)$ differs considerably from the Coulomb potential.

The dynamical equations become

$$\frac{\partial^2 u_n}{\partial t^2} = -G_{n+1} + G_n - F_{n+1} + F_n\,, \tag{1.36}$$

with F_n given by Eq. (1.11) and G_n given by

$$G_n = \frac{\alpha}{1+v_n} \exp\left(-\frac{1+v_n}{\rho}\right)\left(\frac{1}{1+v_n} + \frac{1}{\rho}\right). \tag{1.37}$$

When the joint effect of both the screened Coulomb (ZBL) and bare Coulomb potentials is considered, i.e., Eq. (1.35), numerical simulations show that the behavior of the kinks is not much different from that observed in the bare Coulomb

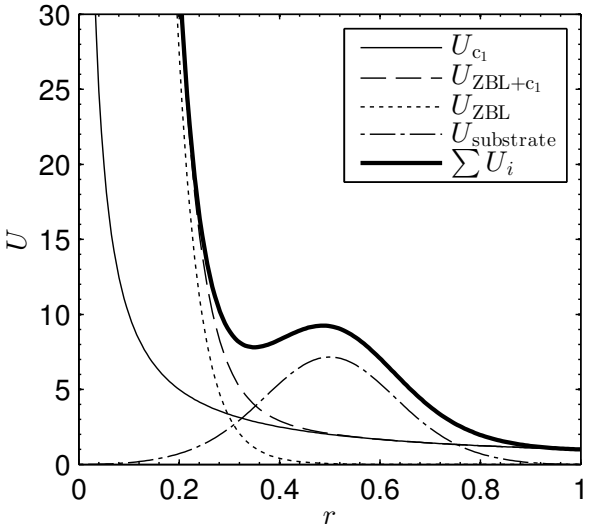


Figure 1.15: Interaction potentials U(r) in dimensionless units. Coulomb (c_1); ZBL (c_{ZBL}); Coulomb+ZBL ($c_{1+\mathrm{ZBL}}$); substrate potential (c_{S}) and the sum of the Coulomb, ZBL and substrate potentials ($c_{1+\mathrm{ZBL}+\mathrm{S}}$). The scaled units are 2.77 eV and the lattice unit a=5.19 Åfor U and r, respectively.

case, discussed in the preceding sections. Supersonic kinks propagate equally well, changing from the magic wavenumber $q = 2\pi/3$ to the proximity of $q = \pi$ and from the sinusoidal to nearly triangular waveform in increasing the amplitude A. Figures 1.13 and 1.14 also show the characteristic curves $V = V(A)$ and $q = q(A)$. The basic difference is that the high energy regime, i.e. the regime of high velocities at witch the waveform change from sinusoidal to triangular, is obtained for for lower (and also realistic) interatomic distances. On the other hand the sound velocity does not change since the ZBL potential is felt only for very large perturbations. Unfortunately, the RWA cannot be obtained analytically but the numerical RWA fits very well the results of the simulations.

1.7 The effect of the substrate potential: lattice kinks or crowdions

In the preceding sections, the interaction with the other atoms in the crystal was taken into account only implicitly, since the only effect of the surrounding atoms was to fix the equilibrium lattice period and to confine the particles within the crystal. To better model the properties of the kinks in a crystal like muscovite, we take into account explicitly the interaction with the surrounding atoms in a simplified mica geometry.

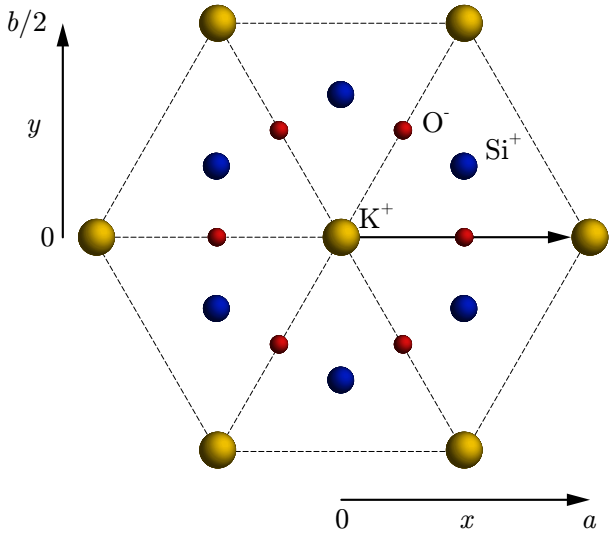


Figure 1.16: Projection on the [001] plane of the ions used in the calculation of the substrate potential. Four planes of ions are considered, two above and two symmetrical below the K^+plane, the closest two with oxygen and the other two with silicon ions. The path for the central K^+ion used the in calculation is shown, note that the O^{-2} ions in the middle of the path are actually at a distance of 1.68Å above and below. The interaction between the K^+ions in the central X-axis is not taken into account in constructing the substrate potential as it is taken into account explicitly. The crystal is continued in the K^+plane until the convergence is achieved. Distance between the longer marks is 1 Å.

The K^+ ions occupy the nodes of the hexagonal lattice with a lattice unit $a = 5.19$ Å. There are no other atoms in the K^+plane, therefore we need to consider more atoms above and below. We consider two planes above and two symmetric below. The closest plane, situated at a height of 1.6795Å, is occupied with oxygen ions with charge -2, their projections on the K^+plane lie in the middle of the two nearest-neighbor K^+ ions. The other layers, at at a height of 2.2227Å from the K^+ plane, are occupied by silicon ions. They are in the centers of tetrahedra whose three horizontal vertices are occupied by the oxygen ions. See the sketch on Fig. 1.16 for a projection of oxygen and silicon layers on the [001] plane, i.e. a top view of the K^+layer. The Si sites are occupied by Si^{+4} and Al^{+3} ions in the proportion of 3:1, giving an average charge of +3.75, but we assign them a smaller charge +2.75 to take into account other atoms in successive layers, particularly the oxygen ions at the top of the tetrahedra, and to achieve charge neutrality.

We suppose that all the atoms are in fixed positions except the moving K^+ ions in a row and only in the [100] direction. This is justified by the supersonic speed of the kinks, that we are interested in, and due to the weak interaction between the Si and Al ions compared to the ZBL interaction between potassium ions when they collide at high velocities. The interaction between the K^+ ions, that are in the central X-axis, are not considered in constructing the substrate potential as

it is taken into account explicitly. The lattice is extended in the [001] K^+ plane until the convergence of the potential is achieved. Specifically the potentials used are the electrostatic interactions and Born-Mayer potentials of the form $V = A\exp(-r/r_g)$, given in Ref. (Gedeon et al., 2002). The value $r_g = 0.29$Å is for all the interactions, and the pre-exponential constants in eV are: $A_{\mathrm{KO}} = 3800.125$, $A_{\mathrm{KSi}} = 2762.5$, $A_{\mathrm{OO}} = 453.375$, $A_{\mathrm{0Si}} = 1851.25$, and $A_{\mathrm{SiSi}} = 1173.125$. For the K^+-K^+ interaction, we use the Coulomb-ZBL potential described above.

We obtain a substrate potential in scaled units ($u_E \simeq 2.77$ eV), which can be described with very good approximation by a truncated Fourier series up to fourth harmonic:

$$U_s(x) = \sum_{h=0}^{4} U_h \cos(2\pi h x) , \tag{1.38}$$

with coefficients U_h equal to [2.4473, -3.3490, 1.0997, -0.2302, 0.0321]. The potential well of 20 eV is consistent with molecular dynamics simulations (Collins et al., 1992). It is represented in Fig. 1.15 together with the other potentials, such that their relative magnitudes can be compared.

1.7.1 Dispersion relations with substrate

Our dynamical equations with a substrate potential $U_s(x)$ in the form given by Eq. (1.38) and for M neighbour Coulomb interactions can be written as

$$\frac{\partial^2 u_n}{\partial t^2} = -\frac{\partial U_s(u_n)}{\partial u_n} + \sum_{m=1}^{M}\left(-\frac{1}{(m+u_{n+p}-u_n)^2} + \frac{1}{(m+u_n-u_{n-m})^2}\right), \tag{1.39}$$

where the restoring forces of the substrate potential are

$$-\frac{\partial U_s(u_n)}{\partial u_n} = \sum_{h=1}^{4} 2\pi h\, U_h \sin(2\pi h u_n) . \tag{1.40}$$

The latter equations, for small amplitude oscillations of u_n becomes

$$-\frac{\partial U_s(u_n)}{\partial u_n} \simeq -\omega_0^2 u_n , \tag{1.41}$$

with the linear frequency ω_0 as

$$\omega_0^2 = \sum_{h=1}^{4} (2\pi h)^2 U_h. \tag{1.42}$$

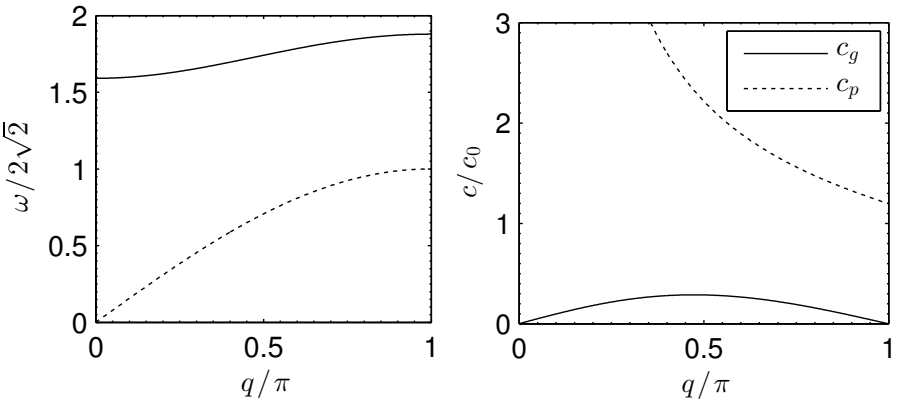


Figure 1.17: Left: Dispersion relation for the linearized Coulomb lattice with (continuous) and without (dotted) substrate potential. Right: Phase (dotted) and group (continuous line) velocity for linearized Coulomb lattice. All dispersion curves are for $M = 1$ neighbour interaction.

The corresponding value for linear frequency is $\omega_0 = 4.48$ or $119\ \mathrm{cm}^{-1}$ in physical units, which is close to $110\ \mathrm{cm}^{-1}$ determined experimentally (Diaz et al., 2000). Therefore the dynamical equations for u_n small become

$$\frac{\partial^2 u_n}{\partial t^2} = -\omega_0^2 u_n + c_0^2 \sum_{m=1}^{M} \frac{1}{m^3} \left(u_{n-m} - 2u_n + u_{n+m}\right) . \tag{1.43}$$

Substitution of $u_n = \exp(\mathrm{i}(qn - \omega t))$ leads to

$$-\omega^2 = -\omega_0^2 + c_0^2 \sum_{m=1}^{M} \frac{1}{m^3} \left(\exp\left(-\mathrm{i}qm\right) - 2 + \exp\left(\mathrm{i}qm\right)\right) . \tag{1.44}$$

Therefore the phonon dispersion relation become

$$\omega^2 = \omega_0^2 + 4\, c_0^2 \sum_{m=1}^{M} \frac{1}{m^3} \sin^2\left(\frac{qm}{2}\right) . \tag{1.45}$$

In the following we particularize for a single neighbour,i.e. $M = 1$. The phonon spectrum becomes an optical one, and the frequency and group velocity are

$$\begin{aligned} \omega^2 &= \omega_0^2 + 4\, c_0^2 \sin^2\left(q/2\right) , \\ c_g &= \frac{\partial \omega}{\partial q} = \frac{c_0^2 \sin q}{\sqrt{\omega_0^2 + 4\, c_0^2 \sin^2\left(q/2\right)}} . \end{aligned} \tag{1.46}$$

Note that c_0 is still the sound speed in the system *without* substrate. Thus, as Fig. (1.17) shows, the dimensionless phonon frequencies ω are in the interval

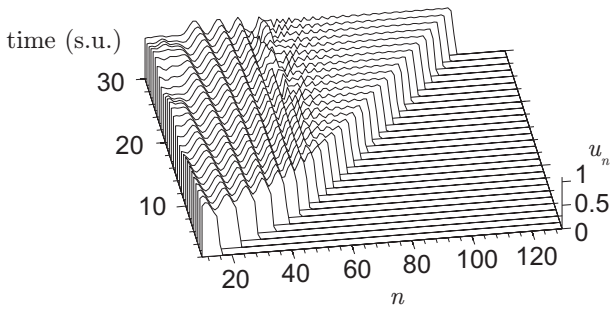


Figure 1.18: Representation of the process of dynamical slowing down of the kink. The nonlinear and linear radiation processes can be easily distinguished. Nonlinear waves with large amplitude are first emitted. Later, the phonons with the wavelength close to $\lambda \simeq 4$, which corresponds to maximal group velocity, and with exponentially decaying amplitudes are emitted while the kink approaches the limit velocity. Scaled units for time and distance are 0.2 ps and lattice constant 5.19 Å.

between $\omega_0 = 4.48$ and $\omega_{\max} = 5.31$. The group velocity is zero at $q = 0$ and $q = \pi$ and reaches its maximum $c_{\mathrm{c,max}} \simeq 0.4$, in the proximity of $q = \pi/2$ with $\lambda \simeq 4$. These features are also observed in the simulations for low amplitude travelling waves.

1.7.2 Qualitative description

The introduction of the substrate potential does not prevent the existence of supersonic lattice kinks. The lattice kink, also called *crowdion*, consists of an interstitial atom propagating very fast in the lattice and leaving behind a vacancy. The specific feature of the kinks found in the present work is that its velocity and energy are fixed by the layer+substrate system, let us denote them as V_c and E_c (c for crowdion). If the initial energy of the excitation is smaller than the threshold E_c, the kinks are rapidly dispersed and disappear and cannot propagate more than few lattice units. However, if it is larger, a kink is formed and its speed depends on its amplitude following the relation $V(A)$ of the ZBL interaction without substrate. However this velocity is not constant with time: the kink always slows down to a fixed stable speed V_c, and the excess energy is backward radiated. The specific values for the stable kink velocity and energy in scaled units are $V_c = 2.7387 \simeq 2c_0$ and $E_c = 9.4374$, corresponding to 7.16 km/s and 26.2 eV, respectively.

The lattice kink is supersonic in the two meanings a) $V_c > c_0$, where c_0 is the sound velocity without substrate; b) V_c is much larger than the maximum phonon group speed $V_{\mathrm{c,max}} \simeq 0.4$ in the system with the substrate, but is not larger than the maximum phase velocity which is unbounded for $q \to 0$, see Fig. (1.17).

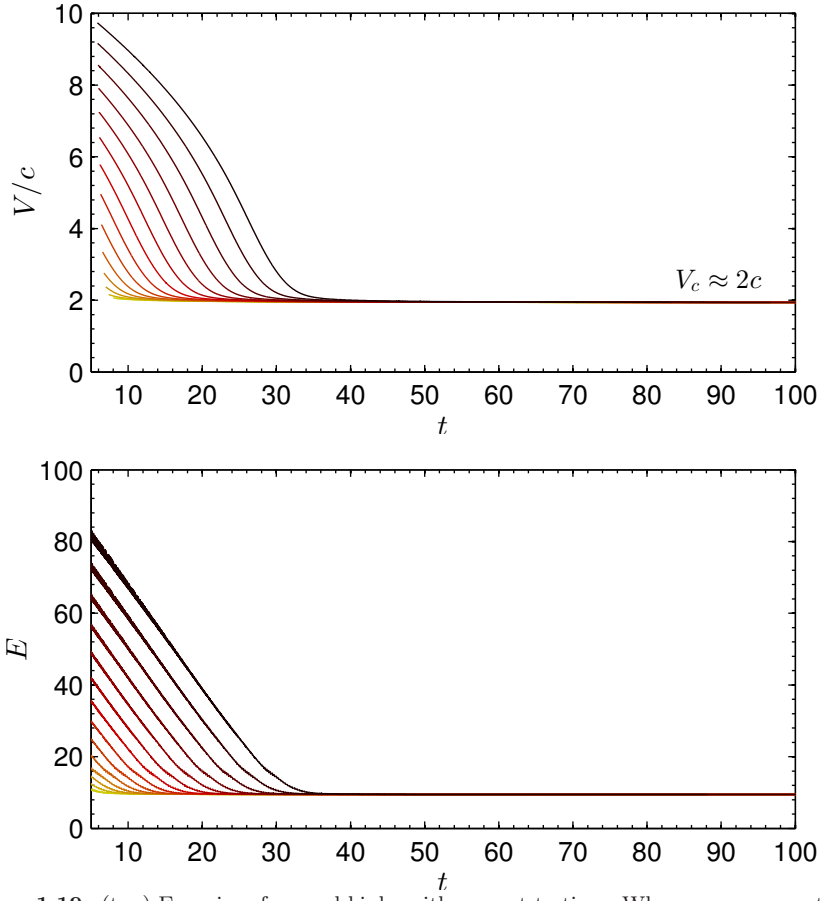


Figure 1.19: (top) Energies of several kinks with respect to time. When more energy than the crowdion's one is delivered a faster kink is produced and a radiation process takes place until the supersonic crowdion is formed. Thereafter, the crowdion is extremely stable. If the initial energy is smaller than the crowdion's one the kink dissipates into phonons. The scaled units are approximately 2.77 eV for energy and 0.2 ps for time. (bottom) Velocities of lattice kinks or crowdions versus time in scaled units for different initial conditions. The final velocity and energy are approached asymptotically, being $V_c = 2.7$ (7.2 km/s) and $E_k = 9.5$ (26.2 eV) in scaled and physical units. For $V < V_c$, the kinks are dissipated into low-amplitude phonons.

1.7.3 Slowing down processes

The process of slowing down to V_c is shown in Figs. (1.18) and (1.19), where two well distinguished phases can be identified.

a) **Nonlinear radiation:** For an initial energy $E > E_c$, the kink progressively loses energy. The particles immediately after the kink perturbation are left with enough energy for nonlinear vibrations in the potential well bringing about

nonlinear wave. Their frequencies obtained numerically are above the phonon band with a maximum value of about 6.3. This strong radiative process is shown in Fig. 1.18 for an initial velocity $V(t=0)=7$. This process is very fast and the decay of kink energy is almost linear with time. As long in this regime the waveform is nearly triangular, kink kinetic energy can be approximated by $K=\frac{1}{2}A^2V^2$ as explained is Sec. (1.4.5). Thus, as the potential energy is negligible for this regime, the linear decay of energy is consistent with the decreasing of velocity at the initial part seen in the of Fig. 1.19.

b) **Linear radiation:** As the lattice kink energy approaches E_c, the amplitude of the tail oscillations and its frequency decrease, the kink frequency enters the phonon band, radiating low amplitude phonons (Braun et al., 1998; Braun et al., 2004). The energy decreases exponentially with time towards E_c. The wave number of the radiated phonons can be deduced from the kink speed as each particle left behind the kink is excited with a delay $\Delta t = 1/V_c$ and, therefore, with a phase difference $q=\omega(q)\Delta t=\omega(q)/V_c$. As the phonon wave vector is given by $q=\omega(q)/c_{\rm ph}$, where $c_{\rm ph}$ is the phase speed of the phonons, $V_{\rm ph}=V_c$. Using the phonon dispersion relation in Eq. (1.46) it is possible to obtain the phonon wavenumber and wavelength $\lambda_{\rm ph}=3.5$ which is the observed one in the simulations. Similar process has been described in Ref. (Braun et al., 1998) and in references therein for subsonic kinks. However, there is an important difference: the subsonic kinks, described in those works, radiate continuously and eventually stop. Here the amplitude of the radiation decreases exponentially, allowing the kink to achieve a constant energy value and propagate stable along the lattice.

From the comparison of Figs. (1.13) and (1.19) with Fig. (1.15) we conclude that supersonic kink's amplitude A of relative particle displacements is determined by the interatomic distance R at the local *minimum* of the combined interatomic plus substrate potential, $R=1-A\approx 0.33$ in lattice units. This value of the kink amplitude ensures the absence of kink oscillations and correspondingly the absence of phonon radiation into the chain by the supersonic kink. We also want to emphasize that we do not observe discrete spectrum (a set of possible values) of the velocity of the supersonic kink in our system, even when we start with high initial kink velocity, see Fig. (1.19). This is in contrast with the prediction of supersonic multi-solitons (lattice N-solitons) in Frenkel-Kontorova model with nonlinear intersite coupling in Refs. (Braun et al., 2004; Savin, 1995; Zolotaryuk et al., 1997). We relate this finding with the extreme discreteness of our kink of effective wavenumber $q\simeq 2\pi/3$, which as shown in Fig. (1.14) corresponds to only two particles moving at a given time, cf. Ref. (Kosevich et al., 2004), which does not allow for different matching with the substrate potential, and also with possible dynamical instability of lattice multi-solitons (bound states of supersonic kinks) in the considered system.

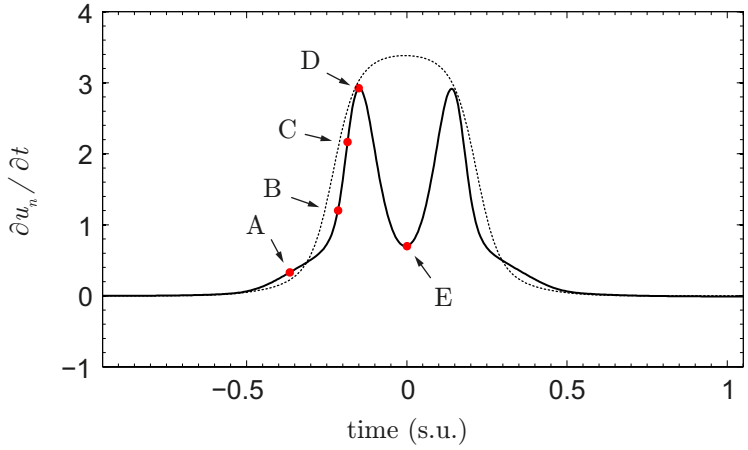


Figure 1.20: Particle velocity waveform measured at $n = 470$ in supersonic kink with amplitude $A = 0.67$ and minimal interatomic distance in lattice units $R = 1 - A = 0.33$ for Coulomb+ZBL potential with (continuous line) and without (dotted line) substrate potential. The instants when the ZBL interaction acts (near A) and the minimum velocity at the top of the potential barrier (E) are easily identified. The configurations at those times can be seen in Fig. 1.21. Scaled units are 0.2 ps and 2.6 km/s.

1.7.4 Double kink

The particle velocity $\dot{u}_n$ as a function of time for the stable kink in the substrate is represented in Fig. 1.20. Due to the extreme discreteness of the kink, it is not practical to represent $\dot{u}_n$ an a function of n. The profile of a double soliton for the particle velocity corresponds to the double kink shown in Fig. (1.21)-(a), is evident as a function of time.

Supersonic multi-solitons in Frenkel-Kontorova system with anharmonic coupling has been described in Refs. (Kosevich et al., 1973; Savin, 1995; Zolotaryuk et al., 1997). They correspond precisely to the discrete set of velocities for which the kinks do not radiate phonons. Although roughly similar in the shape, the kink in our system does not correspond to the mathematical forms obtained in those references. The kink in our system is more discrete, very close to the limit of discreteness, its wavenumber $q \simeq 2\pi/3$, shown in Fig. (1.14), corresponds to only two particles moving at a given time, cf. Ref. (Kosevich et al., 2004).

This discreteness makes possible the exact description of the double kink process as shown in Fig. 1.21 (c): a particle n, represented by a white circle, initially at rest at the bottom of a potential well, experiences two collisions, one when it was hit by the particle $n-1$ and is accelerated afterwards, and a second one when it hits the particle $n+1$ and is decelerated, attaining almost zero velocity at the

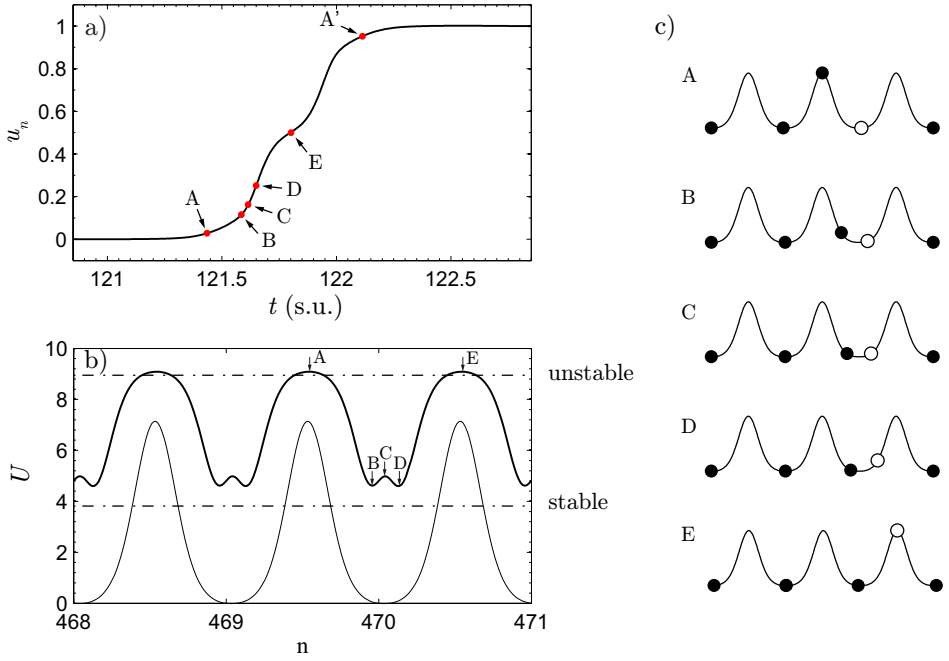


Figure 1.21: (a) Particle displacement waveform for the established lattice kink. (b) Potential energy seen by the kink during propagation (thick line) and periodic substrate potential (thin line), horizontal lines are the energies corresponding to the equilibrium stable (C) and unstable (A) interstitials. (c) Particle configurations corresponding to the points $A-E$, shown in (a) and (b). Scaled units are lattice unit 5.19 Å for distances, 0.2 ps for time and 2.77 eV for energies.

bottom of the potential well (during the radiation process the particle velocity is different from zero). Between the two collisions, the particle finds the substrate potential barrier between sites and experiences a decrease in velocity while going uphill which is followed by an acceleration while going downhill.

Note that the states A and E in Fig. 1.21 have exactly the same energy, but the kink has only moved half a lattice site. This is the first kink of the double-kink process shown in Fig. 1.21 (a). The process of the particle n going downhill and hitting the $n+1$ particle until it stops forms the second kink.

This process can be seen in terms of the kink energy in Fig. 1.21 (b). Two identical oscillations of particle's potential energy U happen for the kink to move a lattice site. There is a local maximum at point C, corresponding to the minimum distance between particles and the short range ZBL interaction. The horizontal dashed-dotted lines indicate the energies for the equilibrium interstitial configurations, with two particles inside a potential well (stable), or one particle at the top of the potential barrier (unstable), with the energy difference corresponding to the Peierls-Nabarro (PN) barrier. The potential energy is always above the stable interstitial energy as the lattice has no time to relax, bringing about an *adi-*

abatic PN barrier. The kink always has finite kinetic energy, with the minimum corresponding to configuration A.

1.8 Some numerical simulations with ultradiscrete kinks or crowdions

In this section we present the results of different simulations to show the capacity of the crowdions to survive a perturbed environment when larger energy is initially delivered and, second, the behaviour of the crowdions with temperature.

1.8.1 Excess energy

We present some examples of simulations when the lattice is given more energy than the 26.2 eV needed to produce the supersonic crowdion. The energies range from 130 eV to 520 eV. They are represented in Fig. 1.22. In (a) a single crowdion is formed after nonlinear waves are emitted. In (b) two crowdions are formed leaving behind an stationary linear wave. Note how the second crowdion survives to the tail of the first and the common velocity V_c of both. In (c) the excessive energy destroys the second crowdion which transforms into a highly localized nonlinear stationary wave. In (d) the second crowdion survives again, while in (e) it is again destroyed. Extensive phonon radiation and wandering kinks can be seen in the latter figure. In (f) a second crowdion survives 150 sites in a highly perturbed media but it is finally pinned down.

1.8.2 Thermalized medium

An interesting question is whether the crowdion can travel trough a previously thermalized medium. This is not only a question of general interest but particulary important for mica muscovite. As it has been calculated in the chapter *Tracks in mica: 50 years later* in this book, the recording process of tracks happens a few kilometers underground under large pressure and temperatures of 700-1000 K. Although much more work is necessary, the answer is positive. For comparison Fig. 1.23 (a-b) shows two simulations at 300 K and 1000 K in the system without substrate potential where the kink survives over hundreds of lattice sites. It is not really surprising as if we compare the energy of the crowdion 26.2 eV with the mean thermal energy of a particle k_BT, the crowdion energy is 1000 and 300 times larger at 300 K and 1000 K respectively.

In the case of including the substrate potential, as shown in Fig. 1.23 (c-d) for 300 K and 1000 K respectively, the crowdion can also travel hundreds of sites of the previously thermalized media. As it was studied in Ref. (Archilla et al.,

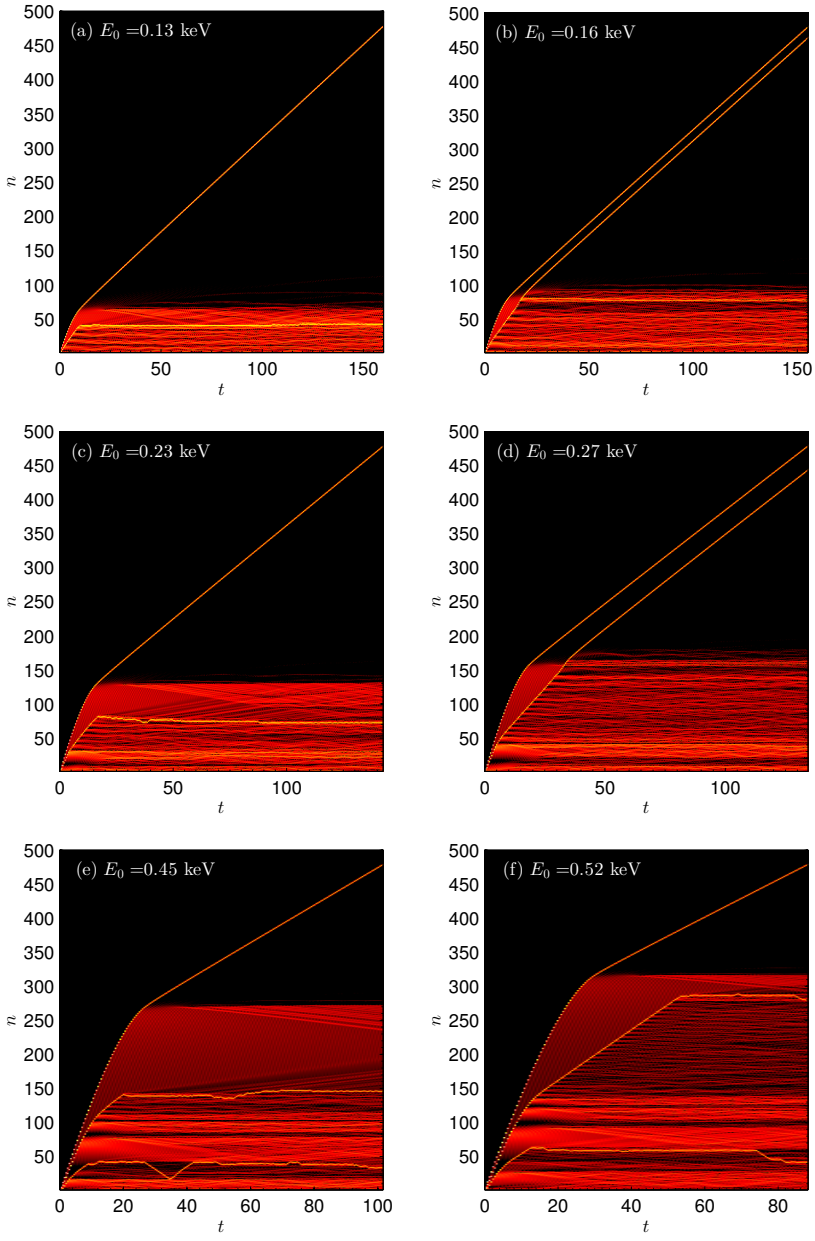


Figure 1.22: (Color) Particle energy plots of several examples of crowdion formation in arbitrary units of $\simeq 3$ eV. Initial energy increases form (a) to (f). Many features can be observed, among them the specific velocity of the crowdion V_c, the formation of nonlinear waves and phonons, the formation of two crowdions and the survival of the crowdion to the severely perturbed media during hundreds of sites

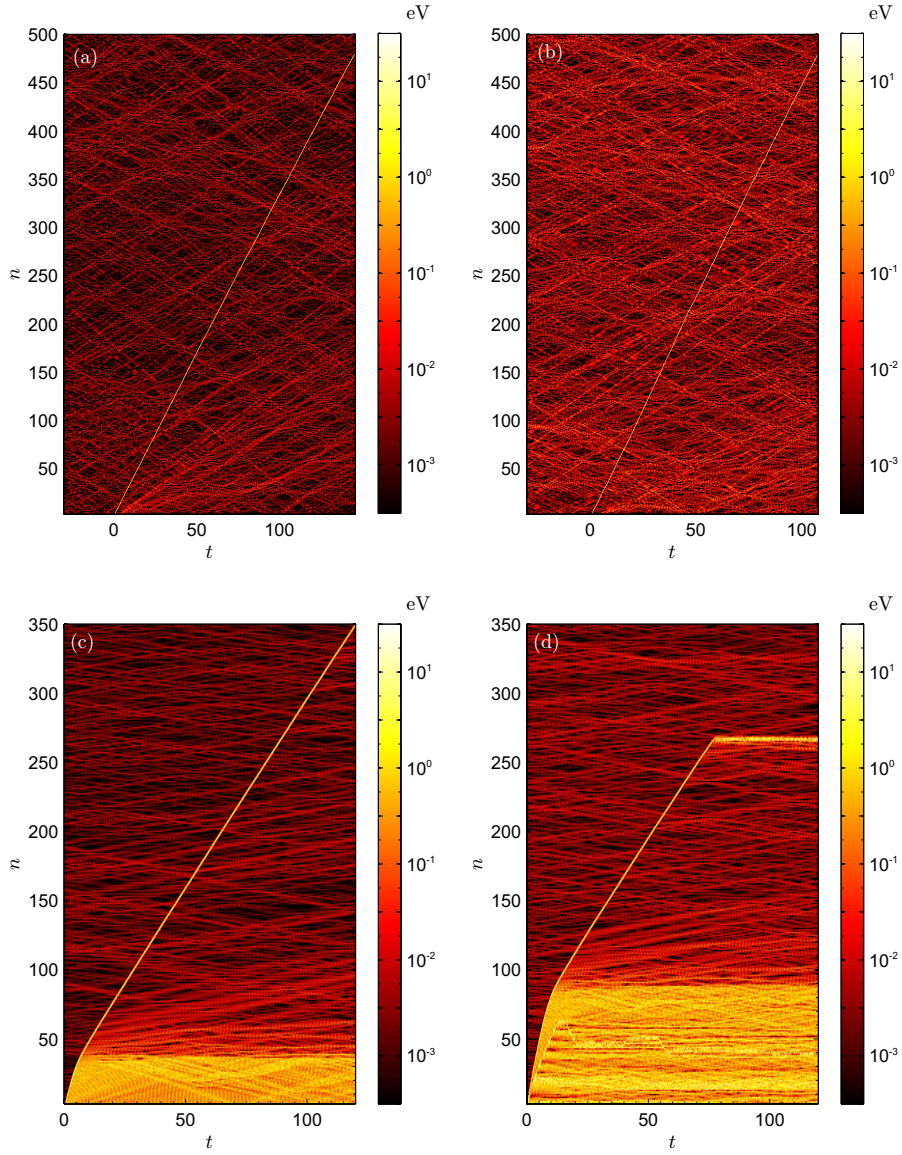


Figure 1.23: (Color) Particle energy plots of two crowdions travelling on a previously thermalized medium at (a,c) 300 K and (b,d) 1000 K, top without and bottom with substrate potential. Color bars are in $10\log_{10}(E)$ units

2015), the crowdion always has finite kinetic energy, but the final total energy of the kink, E_k, is always on the order of magnitude of the Peierls-Nabarro (PN) barrier. The equivalent kinetic energy equivalent for the thermalized media is 0.005

(0.013 eV) at 300 K and 0.016 (0.043 eV) at 1000 K in normalized and physical units . These values are far below the energy difference between the PN barrier and the kink energy. However, in some simulations, for temperatures of 1000 K the thermalization is not completely achieved due to appearance of nonlinear waves instead of phonons. Therefore, localized peaks of the background vibrations can interfere with the crowdion where, in some cases, it can be trapped leading to a highly localized nonlinear stationary perturbation. Figure 1.23 (d) shows and example of this situation, where the crowdion is eventually trapped forming an interstitial defect.

Thermal effects discussed in this section lead to different survival path length of the crowdions. It the hypothesis of crowdions propagating in mica muscovite is correct, they might be related with some the tracks observed in the mineral. Other feature of the presented simulations worth remarking is that the high equivalent temperature of the nonlinear tail radiation of the crowdion is likely to favor a change of structure and the formation of tracks.

1.9 Conclusions

In this chapter we have modeled a low dimensional system using realistic potentials corresponding to a row of ions in a silicate layer, mica muscovite sheet. Our objective was to determine what kind of nonlinear localized modes can exist with realistic parameters and with what characteristics. The choice of the parameters of mica muscovite is motivated by the fact that many of the dark tracks that appear in sheets of this material are consistent with the in-layer propagation of vibrational excitations along close-packed lattice lines of ions, and an experiment has demonstrated that localized energy can travel along lattice directions, being able to eject an atom at the opposite surface.

The modeling of the system has followed a process of increasing complexity to better understand which effect is responsible for which characteristic of the model. In the starting model in preliminary publications (Archilla et al., 2013; Archilla et al., 2014), only K^+ions with nearest-neighbor Coulomb repulsion were present, for which we have found that very fast supersonic kinks can propagate. They are extremely localized, only two particles or for higher energies only a single particle is moving at the same time.

We have added analytical calculations of the energies and compare them with numerical simulations. We have also shown that the introduction of interaction with several neighbours do not produce significant changes as long as the sound speed in each system is taken as a reference. But the extremely short minimal interatomic distances in the kink has motivated the introduction of more realistic short-range ZBL potential. In the improved dynamical model, kinks propagate equally well and with as much energy as desired, but now with realistic minimal

interatomic distances.

The next step was the introduction of a periodic substrate potential using empirical potentials and the geometry of the crystal. Supersonic kinks continue to propagate without losing energy but with several important properties:

a) The main one is that the system selects only one velocity and one energy of the kink;

b) The lattice kink energy is larger than the one which is needed for atom ejection at the surface, and smaller than the one of the proposed sources of energy, the recoil of a K^+ion due to beta emission;

c) The found kinks can be described as the double-kinks or bi-solitons depending of the variable chosen. The unique velocity of the supersonic kink on the periodic substrate potential we relate with the kink amplitude of relative particle displacements which is determined by the interatomic distance corresponding to the minimum of the combined intersite plus substrate potential.

The extreme discreteness of the system with basically two particles moving at the same time allows for the detailed interpretation of the observed double-kinks, which was not possible for multi-kinks without dispersion presented in other works. The double-kink structure is produced by the matching of the two collisions experienced by a particle and the process of going over the substrate potential barrier between neighboring sites. We have shown that realistic potentials allow for the propagation of ultra discrete lattice kinks with energies that are consistent with the properties observed in experiments. Although we cannot claim that those kinks are responsible for those phenomena, it seems likely that they play an important role.

References

Alba, M. D., A. I. Becerro, M. A. Castro, and A. C. Perdigón (2001). "Hydrothermal reactivity of Lu-saturated smectites: Part I. A long-range order study". In: *Amer. Mineral.* 86, p. 115.

Archilla, J. F. R., J. Cuevas, M. D. Alba, M. Naranjo, and J. M. Trillo (2006). "Discrete Breathers for Understanding Reconstructive Mineral Processes at Low Temperatures". In: *J. Phys. Chem. B* 110.47, pp. 24112–24120.

Archilla, J. F. R., Yu. Kosevich, N. Jiménez, V. Sánchez-Morcillo, and L. M. García-Raffi (2013). "Moving Excitations in Cation Lattices". In: *Ucr. J. Phys.* 58.7, pp. 646–656.

Archilla, J. F. R., Yuriy A. Kosevich, N. Jiménez, V. J. Sánchez-Morcillo, and L. M. García-Raffi (2015). "Ultradiscrete kinks with supersonic speed in a layered crystal with realistic potentials". In: *Phys. Rev. E* 91 (2), p. 022912.

Archilla, J.F.R., Y. A. Kosevich, N. Jiménez, V.J. Sánchez-Morcillo, and L.M. García-Raffi (2014). "Supersonic Kinks in Coulomb Lattices". In: *Localized Excitations in Nonlinear Complex Systems*. Ed. by R. Carretero et al. Springer, pp. 317–331.

Biersack, J., J.P. Ziegler, and M.D. Ziegler (2008). *SRIM - The Stopping and Range of Ions in Matter*. Published by J.P. Ziegler.

Braun, O M and Yu S Kivshar (1998). “Nonlinear dynamics of the Frenkel–Kontorova model”. In: *Phys. Rep.* 306, pp. 1–108.

Braun, O.M. and Yu.S. Kivshar (2004). *The Frenkel-Kontorova Model*. Springer.

Brudeylins, G. and D. Schmicker (1995). “Elastic and inelastic helium atom scattering at a cleaved mica sheet.” In: *Surf. Sci.* 333, pp. 237–242.

Chaikin, P. M. and T. C. Lubensky (1995). *Principles of Condensed Matter Physics*. Cambridge: Cambridge University Press, pp. 601–602.

Chaplot, SL and et al (2002). “Inelastic neutron scattering and lattice dynamics of minerals”. In: *Eur. J. Min.* 14, p. 291.

Collins, D R and C R A Catlow (1992). “Computer simulation of structure and cohesive properties of micas”. In: *Am. Min.* 77, pp. 1172–1181.

Collins, D.R., W.G. Stirling, C.R.A. Catlow, and G. Rowbotham (1993). “Determination of Acoustic Phonon Dispersion Curves in Layer Silicates by Inelastic Neutron Scattering and Computer Simulation Techniques.” In: *Phys. Chem. Miner.* 19, pp. 520–527.

Diaz, M, V. C. Farmer, and R Prost (2000). “Characterization and assignment of far infrared absorption bands of K^+ in muscovite”. In: *Clays Clay Miner.* 48, pp. 433–438.

Dou, Q., J. Cuevas, J. C. Eilbeck, and F. M. Russell (2011). “Breathers and kinks in a simulated crystal experiment”. In: *Discret. Contin. Dyn. S.-S* 4, pp. 1107–1118.

Dubinko, V. I., P. A. Selyshchev, and J. F. R. Archilla (2011). “Reaction-rate theory with account of the crystal anharmonicity”. In: *Phys. Rev. E* 83, p. 041124.

Durrani, S. A. (2001). “Nuclear tracks: A success story of the 20th century”. In: *Rad. Meas* 34, pp. 5–13.

Durrani, S. A. (2008). “Nuclear tracks today: Strengths, weaknesses, challenges”. In: *Rad. Meas* 43, S26–S33.

Fleischer, R.L. (2011). *Tracks to Innovation. Nuclear Tracks in Science and Technology*. Springer.

Frenkel, Ya. and T. Kontorova (1938). “-”. In: *Phys. Z. Sowjetunion* 13 (1), p. 1.

Friesecke, G. and K. Matthies (2002). “Atomic-scale localization of high-energy solitary waves on lattices”. In: *Physica D* 171.4, pp. 211 –220.

Gedeon, O., J. Machacek, and M. Liska (2002). “Static energy hypersurface mapping of potassium cations in potassium silicate glasses”. In: *Phys. Chem. Glass.* 43.5, pp. 241–246.

Hong, Z. L., H. Yoshida, Y. Ikuhara, T. Sakuma, T. Nishimura, and M. Mitomo (2002). “The effect of additive on sintering behavior and strength retention in silicon nitride with RE-disilicate”. In: *J. Eur. Ceram. Soc.* 22, p. 527.

Kosevich, A.M. and A.S. Kovalev (1973). “The supersonic motion of a crowdion. The one dimensional model with nonlinear interaction between the nearest neighbors”. In: *Solid State Commun.* 12, pp. 763–764.

Kosevich, Yu. A. (1993). “Nonlinear sinusoidal waves and their Superposition in anharmonic lattices.” In: *Phys. Rev. Lett.* 71, pp. 2058–2061.

Kosevich, Yu. A., R. Khomeriki, and S. Ruffo (2004). “Supersonic discrete kink-solitons and sinusoidal patterns with *magic* wave number in anharmonic lattices”. In: *Europhys. Lett.* 66, pp. 21–27.

Kudriavtsev, Y., A. Villegas, A. Godines, and R. Asomoza (2005). “Calculation of the surface binding energy for ion sputtered particles”. In: *Appl. Surf. Sci.* 239.3-4, pp. 273–278.

Milchev, Andrey (1990). “Breakup threshold of solitons in systems with nonconvex interactions”. In: *Phys. Rev. B* 42 (10), pp. 6727–6729.

Molerón, M., A. Leonard, and C. Daraio (2014). “Solitary waves in a chain of repelling magnets”. In: *J. Appl. Phys.* 115.18, p. 184901.

Ni, Y, Yu A. Kosevich, S. Xiong, Y. Chalopin, and S. Volz (2014). “Substrate-induced cross-plane thermal propagative modes in few-layer graphene”. In: *Phys. Rev. B* 89 (20), p. 205413.

Price, P. B. and R. M. Walker (1962). “Observation of fossil particle tracks in natural micas”. In: *Nature* 196, pp. 732–734.

Russell, F. (1988a). “Identification and selection criteria for charged lepton tracks in mica”. In: *Nucl. Tracks. Rad. Meas.* 15, pp. 41–44.

Russell, F. M. (1967a). “Duration of sensitive period for track recording in mica”. In: *Nature* 217, pp. 51–52.

Russell, F. M. (1967b). “Tracks in mica caused by electron showers”. In: *Nature* 216, pp. 907–909.

Russell, F. M. (1988b). "Positive charge transport in layered crystalline solids". In: *Phys. Lett. A* 130, pp. 489–491.
Russell, F. M. and J. C. Eilbeck (2007). "Evidence for moving breathers in a layered crystal insulator at 300K". In: *Europhys. Lett.* 78, p. 10004.
Savin, A. V. and Yu A. Kosevich (2014). "Thermal conductivity of molecular chains with asymmetric potentials of pair interactions". In: *Phys. Rev. E* 89 (3), p. 032102.
Savin, A.V. (1995). "Supersonic regimes of motion of a topological soliton". In: *Sov. Phys. JETP* 81, pp. 608–613.
Schlößer, D., K. Kroneberger, M. Schosnig, F. M. Russell, and K. O. Groeneveld (1994). "Search for solitons in solids". In: *Rad. Meas* 23, pp. 209–213.
Silk, E C H and R S Barnes (1959). "Examination of fission fragment tracks with an electron microscope". In: *Phylos. Mag.* 4, pp. 970–971.
Snowden-Ifft, D. P., E. S. Freeman, and P. B. Price (1995). "Limits on dark-matter using ancient mica". In: *Phys. Rev. Lett.* 74.21, pp. 4133–4136.
Wada, N and WA Kamitakahara (1991). "Inelastic neutron and Raman scattering studies of muscovite and vermiculite layered silicates." In: *Phys. Rev. B* 43, p. 2391.
Zolotaryuk, Y., J.C Eilbeck, and A.V. Savin (1997). "Bound states of lattice solitons and their bifurcations". In: *Physica D* 108, pp. 81–91.

Publications

The contents of this chapter has been presented in the following publications:

Journal papers

- Archilla, J. F., Kosevich, Y. A.; **Jiménez, N.**, Sánchez-Morcillo, V. and García-Raffi, L. M. "Ultradiscrete kinks with supersonic speed in a layered crystal with realistic potentials" *Phys. Rev. E*, 91, 022912 (2015)
- Archilla, J. F., Kosevich, Y. A., **Jiménez, N.**, Sanchez-Morcillo, V. and García-Raffi, L. M. "Moving excitations In cation lattices" *Ukranian Journal of Physics*, 58, 646-656 (2013)

Conference proceedings

- **Jiménez, N.**, Archilla, J. F., Kosevich, Y. A., Sanchez-Morcillo, V. and García-Raffi, L. M. "A crowdion in mica. Between K40 recoil and transmission sputtering" *Quodons in mica: nonlinear localized travelling excitations in crystals*, Altea, Spain. September 18-21, (2013)
- **Jiménez, N.**, Sánchez-Morcillo, V., García-Raffi, L. M. and Archilla, J. F. "Kinks supersónicos en redes repulsivas" *XXXIV Reunión Bienal de la Real Sociedad Española de Física*, Valencia, Spain. July 17, (2013)
- Archilla, J. F., Kosevich, Y. A., **Jiménez, N.**, Sanchez-Morcillo, V. and García-Raffi, L. M. "Effect of ZBL potential on kinks in repulsive lattices" *IV International Symposium on Strong Nonlinear Vibronic and Electronic Interactions in Solids*. Tartu, Estonia, May 1-3, (2013)

- Archilla, J. F., Kosevich, Y. A., **Jiménez, N.**, Sanchez-Morcillo, V. and García-Raffi, L. M. "Moving excitations in cation lattices" *Problems of theoretical physics* (dedicated to the 100th anniversary of Alexander Davydov). Kiev, Ukraine, October 8-11, (2012)
- Archilla, J. F., Kosevich, Y. A., **Jiménez, N.**; Sanchez-Morcillo, V. and García-Raffi, L. M. "Supersonic solitons and kinks in repulsive lattices" *Lattice Solitons and Irradiation-Induced Nonlinear Phenomena in Solids*. Tartu, Estonia, October 31-November 2, (2012)

Book chapters

- Carretero-González, R. & others (Eds.) **Localized Excitations in Nonlinear Complex Systems**, Springer (2014). Archilla, Juan F. R. and Kosevich, Yuriy A. and **Jiménez, Noé** and Sánchez-Morcillo, Víctor J. and García-Raffi, Luís M. "Supersonic Kinks in Coulomb Lattices", pp. 317-331 (2014),
- L. M. Archilla, J. F. R.; **Jiménez, N.**; Sánchez-Morcillo, V. J. & García-Raffi, L. M. (Eds.) **Quodons in mica: nonlinear localized travelling excitations in crystals**, Springer, (2015). Archilla, J. F., Kosevich, Y. A., **Jiménez, N.**, Sanchez-Morcillo, V. and García-Raffi, L. M. " A supersonic crowdion in mica: Ultradiscrete kinks with energy between $K^4 0$ recoil and transmission sputtering", pp 69–98 (2015).